NASA TECHNICAL MEMORANDUM

NASA TM X-2642

NASA TM X-2642

HYPERSONIC AEROTHERMAL CHARACTERISTICS OF A MANNED LOW-FINENESS-RATIO SHUTTLE BOOSTER

by Peter T. Bernot and David A. Throckmorton

Langley Research Center
Hampton, Va. 23365

NATIONAL AERONAUTICS AND SPACE ADMINISTRATION • WASHINGTON, D. C. • NOVEMBER 1972

1. Report No.	2. Government Accession No.	3. Recipient's Catalog No.
NASA TM X-2642		

4. Title and Subtitle	5. Report Date
HYPERSONIC AEROTHERMAL CHARACTERISTICS OF A MANNED LOW-FINENESS-RATIO SHUTTLE BOOSTER	November 1972
	6. Performing Organization Code

7. Author(s)	8. Performing Organization Report No.
Peter T. Bernot and David A. Throckmorton	L-8453
	10. Work Unit No.
9. Performing Organization Name and Address	502-37-01-06
NASA Langley Research Center Hampton, Va. 23365	11. Contract or Grant No.
	13. Type of Report and Period Covered
12. Sponsoring Agency Name and Address	Technical Memorandum
National Aeronautics and Space Administration Washington, D.C. 20546	14. Sponsoring Agency Code

15. Supplementary Notes

16. Abstract

An investigation of a winged booster model having canards and an ascent configuration comprised of the booster mounted in tandem with an orbiter model has been conducted at Mach 10.2 in the Langley continuous-flow hypersonic tunnel. Longitudinal and lateral-directional force characteristics were obtained over angle-of-attack ranges of -12° to 60° for the booster and -11° to 11° for the ascent configuration. Interference heating effects on the booster using the phase-change coating technique were determined at 0° angle of attack. Some oil-flow photographs of the isolated booster and orbiter and ascent configuration are also presented.

17. Key Words (Suggested by Author(s))	18. Distribution Statement
Space vehicles Shuttle booster Shuttle-launch configuration Aeronautical stability Heat transfer	Unclassified – Unlimited

19. Security Classif. (of this report)	20. Security Classif. (of this page)	21. No. of Pages	22. Price*
Unclassified	Unclassified	44	$3.00

*For sale by the National Technical Information Service, Springfield, Virginia 22151

HYPERSONIC AEROTHERMAL CHARACTERISTICS OF A MANNED LOW-FINENESS-RATIO SHUTTLE BOOSTER

By Peter T. Bernot and David A. Throckmorton
Langley Research Center

SUMMARY

Wind-tunnel tests have been conducted at Mach 10.2 to determine longitudinal and lateral-directional characteristics of a booster model and an ascent configuration which was comprised of the booster and an orbiter arranged in tandem. Heat-transfer tests on the booster were also performed to ascertain interference effects due to the presence of the orbiter. Booster heating rates and wall-temperature response were computed for a nominal trajectory.

The booster could be trimmed at the planned entry angle of 60° with the canards alined to the flow. Although the booster is directionally unstable at this attitude, a positive dihedral effect and $C_{n_{\beta,dyn}}$ assure an oscillatory response to directional disturbances. At low angles of attack, the booster pitch-up may facilitate transition to the high entry attitude. Lateral stability was achieved; however, the vertical tail, because of a short moment arm, was ineffective in providing directional stability even at low angles of attack. The ascent configuration was stable about all three axes over the operational angle-of-attack range, with configuration drag less than half of that measured for the booster alone. Interference effects on the booster heating during ascent flight were small. Calculated heat load on the booster over the complete trajectory indicated that the heat-sink concept using aluminum was feasible for the estimated staging velocity of 2350 meters per second.

INTRODUCTION

During the early phases of space shuttle concept definition, a low-fineness-ratio booster designed for tandem mounting with a fully reusable orbiter was tested at the Langley Research Center. When compared with piggyback shuttle concepts, this system offered promise in reducing structural weight, ascent drag, and interference heating. The booster configuration incorporated a cylindrical fuselage with horizontal canard surfaces, a low wing, and a vertical tail. Longitudinal and lateral-directional characteristics of the booster alone were obtained over an angle-of-attack range from -12° to 60°; data were

also obtained on the ascent configuration comprised of a delta-wing orbiter mounted ahead of the booster over an angle-of-attack range of -11° to 11°. The test results are compared with theoretical estimates of booster-alone characteristics.

The feasibility of an aluminum heat sink for booster thermal protection was investigated with the booster and orbiter sized for staging at relatively low velocities. Transient wall-temperature response for points on the fuselage windward center line and along wing spanwise rays was calculated for a nominal trajectory with staging at 2350 meters/second, followed by a high angle-of-attack return. Effects of orbiter-booster proximity on ascent heating were determined experimentally.

All tests were made in the Langley continuous-flow hypersonic tunnel at a Mach number of 10.2 and a Reynolds number of approximately 0.73×10^6 based on booster model length.

SYMBOLS

The longitudinal characteristics are referred to the body- and stability-axis systems; the lateral-directional characteristics are based on the body-axis system. The moment reference point for the booster configurations was located at 74.8 percent of fuselage length and 1.7 percent below model center line. For the ascent configuration, the moment reference point at 6.1 percent rearward of the booster nose and 0.95 percent below the center line represents the calculated center-of-gravity location just prior to staging.

b	wing span, centimeters
C_A	axial-force coefficient, $\frac{\text{Axial force}}{qS}$
C_D	drag coefficient, $\frac{\text{Drag}}{qS}$
C_L	lift coefficient, $\frac{\text{Lift}}{qS}$
C_l	rolling-moment coefficient, $\frac{\text{Rolling moment}}{qSb}$
C_{l_β}	lateral stability parameter, $\frac{\Delta C_l}{\Delta \beta}$, per degree

C_m pitching-moment coefficient, $\frac{\text{Pitching moment}}{qS\ell}$

C_N normal-force coefficient, $\frac{\text{Normal force}}{qS}$

C_n yawing-moment coefficient, $\frac{\text{Yawing moment}}{qSb}$

C_{n_β} directional stability parameter, $\frac{\Delta C_n}{\Delta \beta}$, per degree

$C_{n_{\beta,dyn}} = C_{n_\beta} \cos \alpha - \frac{I_Z}{I_X} C_{\ell_\beta} \sin \alpha$, per degree

C_p pressure coefficient

C_Y side-force coefficient, $\frac{\text{Side force}}{qS}$

C_{Y_β} side-force parameter, $\frac{\Delta C_Y}{\Delta \beta}$, per degree

c_r reference wing chord, meters (see fig. 10)

d model fuselage diameter, meters

h heat-transfer coefficient

$\frac{I_Z}{I_X}$ ratio of moments of inertia based on model axis system

L/D lift-drag ratio, $\frac{C_L}{C_D}$

ℓ fuselage length, meters

M_∞ free-stream Mach number

M_e Mach number at edge of boundary layer

q free-stream dynamic pressure, newtons/meter^2

$\dot{q}$ heating rate, watts/meter^2

$R_{\infty,d}$ free-stream Reynolds number based on fuselage diameter

$R_{e,x}$ Reynolds number based on local conditions and axial distance

$R_{e,\theta}$ Reynolds number based on local conditions and boundary-layer momentum thickness

S theoretical wing planform area, centimeters^2

T temperature, kelvins

t time, seconds

x axial distance measured parallel to model reference center line

α angle of attack, degrees

β angle of sideslip, degrees

δ_c canard deflection, positive for trailing edge down, degrees

δ_e elevon deflection, positive for trailing edge down, degrees

ϕ transition parameter, $\dfrac{R_{e,\theta}/M_e}{(R_{e,x}/x)^{0.2}}$

Subscripts:

r=1 conditions at stagnation point of a sphere having a radius of 0.3048 meter (1 ft)

ref conditions at stagnation point of a sphere scaled to model size from a full-scale radius of 0.3048 meter (1 ft)

max maximum

Model component designations:

B fuselage (body of revolution with canopy)

C canards

V vertical tail

W wing

APPARATUS AND MODELS

The continuous-flow hypersonic tunnel is a closed-circuit facility with a 78.7-centimeter- (31-in.-) square test section. To prevent liquefaction, air is heated to approximately 1055 K by use of electrical resistance tube bundles. (See ref. 1 for a more detailed list of operational characteristics.) Force and moment data were measured by a water-cooled six-component strain-gage balance which was connected to a remotely controlled strut mechanism. The entire balance-strut assembly was mounted on an injection mechanism that permitted model insertion into the hot airstream from a cooling chamber located adjacent to the test section (see ref. 2). The phase-change coating technique (refs. 3 and 4) was used to determine interference heat transfer.

The booster model (fig. 1) had a fuselage fineness ratio of 4.07 and a length of 22.62 centimeters (8.90 in.); the wing had an overall aspect ratio of 3.6 and employed an NACA 0012-64 airfoil at 0° incidence. The force model was machined from metal and incorporated full-span elevons having a deflection range up to -45°; the vertical tail employed a 6° wedge section with a blunted leading edge and flat base. The all-movable canards were configured to avoid porting between the canard forebody and the fuselage as they were deflected. The ascent configuration consisted of a 25.4-centimeter- (10-in.-) long aluminum model of the North American Rockwell 134-D delta-wing orbiter attached in tandem to the booster model by means of a 0.635-centimeter- (0.25-in.-) diameter rod. (See fig. 2.) Photographs of the test models are presented in figure 3. A similar booster model, constructed of castable resin, was used in ascent heating studies.

RESULTS AND DISCUSSION

Aerodynamic Characteristics

Booster alone.- Component-breakdown data for the booster alone (fig. 4) are compared with estimates using the method of reference 5 where modified Newtonian theory $\left(C_{p,max} = 1.833\right)$ was applied to the body and tangent-cone theory on the wing, canards, and vertical tail. Prandtl-Meyer expansion was used on the shadowed regions; skin-friction effects were not included. For the body alone, predictions of C_L, C_D, and L/D were reasonably good; C_m was overestimated although the trend with angle of attack was quite good. Theory gave good predictions of the lateral-directional charac-

teristics. For the body-wing configuration, theory again compared favorably with the measured forces whereas prediction of C_m was not good. Addition of the wing gave no improvement to directional stability; this result was predicted by theory. Experiment showed large increases in positive dihedral effect $\left(-C_{l_\beta}\right)$ as angle of attack increased to 60^o where the measured value was almost twice that predicted. For the body-canard-wing configuration with $\delta_c = -60^o$, the measured pitching moments were in better agreement with theory than for the body-wing configuration; C_L, C_D, and L/D were also in good agreement. The lateral-directional parameters were only slightly affected by the addition of the deflected canards. Theory again gave good predictions for C_{n_β} and C_{Y_β} and a sizable underprediction for C_{l_β} at the higher angles of attack.

The effects of elevon deflection for hypersonic entry conditions with the canards set at -60^o are presented in figure 5. Results of extrapolations of pitching-moment versus elevon-deflection data resulted in the dashed curves of figure 5(a) and indicated that the booster can be trimmed at the planned entry angle of attack of 60^o for an elevon deflection of approximately 3.5^o. Trim values of C_L and L/D were 0.89 and 0.5, respectively. The effective dihedral was positive throughout the test angle-of-attack range; and although the booster was directionally unstable, calculations indicated that $C_{n_{\beta,dyn}}$ was positive for realistic values of moment of inertia at high angle of attack.

The canard effectiveness (fig. 6) indicates that the booster cannot be trimmed for the calculated moment center. Although directional stability is decreased and lateral stability is increased with decreasing canard deflection, these effects are small.

Data for the complete booster over the low angle-of-attack range are presented in figure 7 and represent the booster immediately after staging. Although longitudinal instability might require augmentation, the pitch-up occurring as angle of attack is increased could be desirable in rotating the booster to its high angle-of-attack turn-around and entry attitude. Theory gave fair agreement with experimental L/D although C_D was somewhat underestimated; excellent agreement with experimental C_m is seen at angles of attack up to 14^o. Lateral stability was obtained at positive angles of attack; however the vertical tail failed to provide directional stability. Prediction of C_{n_β} and C_{Y_β} was generally good while the trend in measured C_{l_β} was poorly predicted.

In general, theory yielded reasonable agreement with the measured forces but was somewhat unreliable in predicting the moments. This result was anticipated from previous experience with this theory.

Ascent configuration.- The aerodynamic characteristics of the ascent configuration are presented in figure 8 and this configuration is seen to be stable about all three axes for the angle-of-attack range of interest. It is noted that the drag of the booster-orbiter combination is less than half of that obtained on the booster alone near zero lift.

Heat Transfer

Convective heat transfer to lower surface body and wing reference points was computed along a nominal trajectory (fig. 9) with a zero lift boost to staging at approximately 2350 meters/second and return at $\alpha = 60^{\circ}$ through the heat pulse. Geometric locations of the body reference points and wing reference lines are indicated in figure 10.

The flow models used for these computations are summarized in table I.

TABLE I.- COMPUTATIONAL FLOW MODELS

	Body points for ascent	Body points for return	Wing points
Heat transfer:			
Laminar	Eckert reference enthalpy (ref. 6)	Modified Beckwith and Gallagher swept cylinder (ref. 8)	Eckert reference enthalpy (ref. 6)
Turbulent	Spalding and Chi (ref. 7)	Modified Beckwith and Gallagher swept cylinder (ref. 8)	Spalding and Chi (ref. 7)
Transition:			
Laminar	$R_{e,x} < 500$ K	$R_{\infty,d} < 100$ K	$\phi < 12$
Transitional	500 K $< R_{e,x} <$ 1000 K	100 K $< R_{\infty,d} <$ 200 K	$12 < \phi < 18$
Turbulent	1000 K $< R_{e,x}$	200 K $< R_{\infty,d}$	$18 < \phi$
Shock-wave angle . . .	Normal	Parallel to body	Conical
Pressure	Modified Newtonian	Swept cylinder	Tangent-cone

For body points, flat-plate theories were used for ascent-phase computation, and swept-cylinder theory was applied during the high angle-of-attack return. Heating to the wing reference lines was based on flat-plate theory for the complete trajectory.

When the transition criteria indicated the boundary-layer state to be either laminar or turbulent, the appropriate theory was used to compute the local heat-transfer rate. However, if the criteria indicated a transitional boundary layer, heat transfer was taken as a weighted average of the laminar and turbulent values.

Computed heat-transfer rates to the two body points (fig. 11) are approximately equal over the entire trajectory. With the assumed transition criteria, the peak heating pulse during entry occurs at a time when the boundary layer is turbulent. The integrated heat load for the ascent portion of the flight is shown to represent only a small fraction of the total heat load for the complete trajectory.

Based upon computed heating rates, radiative cooling (emissivity of 0.85), and thermophysical properties for aluminum, the transient skin-temperature response was computed at both fuselage stations for several skin thicknesses (fig. 12). Since the strength characteristics of aluminum alloys degrade rapidly at material temperatures above 450 K, it is apparent that a skin thickness approaching 1.25 centimeters would be required for an aluminum heat sink to be used. Transient skin-temperature-response data for the wing (fig. 13) are based upon the use of a 0.076-centimeter thickness of René 41. From the standpoint of thermal-strength degradation, wing skins of still lesser thickness may be used inasmuch as this material has a critical temperature limit of approximately 1100 K. Boost-phase temperature increases are again small, and skin temperatures tend to follow local recovery temperatures following the peak heating pulse.

For the purpose of these calculations, it was assumed that heating to the booster was not influenced by the flow field associated with the orbiter. As a check of the validity of this assumption, heat transfer to the booster in the presence of the orbiter (fig. 2) was measured at $M_\infty = 10.2$ by the phase-change-coating technique (refs. 3 and 4). The data are presented (fig. 14) in the form of lines of constant heat-transfer coefficient normalized by the stagnation point value for a scaled 0.3048-meter- (1-ft-) radius sphere under tunnel test conditions. While these contours identify heating gradients over the body, which are a result of the interference aerodynamics, the magnitude of heating rates experienced by the majority of the surface area are of the same order of magnitude as those experienced by the booster in the undisturbed stream. In view of the small contribution of ascent heating to the vehicle total heat load and the absence of large heating magnification due to orbiter-booster aerodynamics, it is clear that interference heat transfer during ascent does not significantly impact body surface temperature.

Surface Flow Fields

Oil-flow photographs of the ascent configuration and of the isolated orbiter and booster at zero angle of attack are presented in figure 15. The top and side views show strong shielding of the booster fuselage by the orbiter. This is especially clear in the top view (fig. 15(b)) where the presence of the orbiter eliminated much of the scrubbing action on the booster nose and resulted in apparent reduction of the vortex action on the upper surface. In the bottom view (fig. 15(c)), three impingement regions are discernible on the booster nose and correlate with the heating rates observed in figure 14(b). The shielding of the booster by the orbiter not only reduces heating over much of the fuselage but is also the source of gross-drag reductions.

Oil-flow photographs of the booster model at 60° angle of attack with the canards alined with the flow (fig. 16) clearly show the similarity to flow on swept cylinders; this similarity supports the use of swept-cylinder theory in calculating heating on the fuselage.

The curvature of the separation lines caused by the wing are clearly shown in the side view. The stagnation point occurring on the nose (figs. 16(a) and (c)) appears to be located just ahead of the canard.

CONCLUSIONS

A wind-tunnel investigation was conducted at the Langley Research Center on a two-stage tandem shuttle concept at Mach 10.2. Longitudinal and lateral-directional stability characteristics were obtained for a low-fineness-ratio booster and an ascent (launch) configuration which incorporated a delta-wing orbiter. Interference effects on booster heating due to presence of the orbiter were also determined experimentally. The results indicated the following conclusions:

1. Based upon extrapolation of elevon effectiveness data, the booster was trimmable at the planned entry angle of 60° with the canards alined to the flow. The configuration displayed positive effective dihedral and, although directionally unstable, the positive values of $C_{n_{\beta,dyn}}$ at high angle of attack assure an oscillatory response to directional disturbances.

2. At low angles of attack, the booster exhibited pitch-up which could be desirable in order to achieve its high entry attitude. The vertical tail failed to provide directional stability; however, lateral stability was satisfactory.

3. The ascent configuration had three-axis stability over the angle-of-attack range of interest. The drag for this configuration was less than half of that measured for the booster alone.

4. Interference effects on the booster heat transfer during ascent were determined experimentally and were found to be small. Calculated booster heat load during ascent flight represented only a small fraction of the total heat load over the complete trajectory.

5. From the heating standpoint, the aluminum heat-sink concept for booster thermal protection appears feasible.

Langley Research Center,
National Aeronautics and Space Administration,
Hampton, Va., October 10, 1972.

REFERENCES

1. Schaefer, William T., Jr.: Characteristics of Major Active Wind Tunnels at the Langley Research Center. NASA TM X-1130, 1965.

2. Dunavant, James C.; and Stone, Howard W.: Effect of Roughness on Heat Transfer to Hemisphere Cylinders at Mach Numbers 10.4 and 11.4. NASA TN D-3871, 1967.

3. Jones, Robert A.; and Hunt, James L.: Use of Fusible Temperature Indicators for Obtaining Quantitative Aerodynamic Heat-Transfer Data. NASA TR R-230, 1966.

4. Throckmorton, David A.: Heat-Transfer Testing Procedures in Phase B Shuttle Studies With Emphasis on Phase-Change Data Improvement. Space Shuttle Aerothermodynamics Technology Conference, Vol. II, NASA TM X-2507, 1972, pp. 661-682.

5. Gentry, Arvel E.: Hypersonic Arbitrary-Body Aerodynamics Computer Program. Vol. I – User's Manual. Rep. DAC 56080, Douglas Aircraft Co., Mar. 1967. (Available from DDC as AD 817 158.)

6. Eckert, Ernst R. G.: Survey of Boundary Layer Heat Transfer at High Velocities and High Temperatures. WADC Tech. Rep. 59-624, U.S. Air Force, Apr. 1960.

7. Spalding, D. B.; and Chi, S. W.: The Drag of a Compressible Turbulent Boundary Layer on a Smooth Flat Plate With and Without Heat Transfer. J. Fluid Mech., vol. 18, pt. 1, Jan. 1964, pp. 117-143.

8. Beckwith, Ivan E.; and Gallagher, James J.: Local Heat Transfer and Recovery Temperatures on a Yawed Cylinder at a Mach Number of 4.15 and High Reynolds Numbers. NASA TR R-104, 1961. (Supersedes NASA MEMO 2-27-59L.)

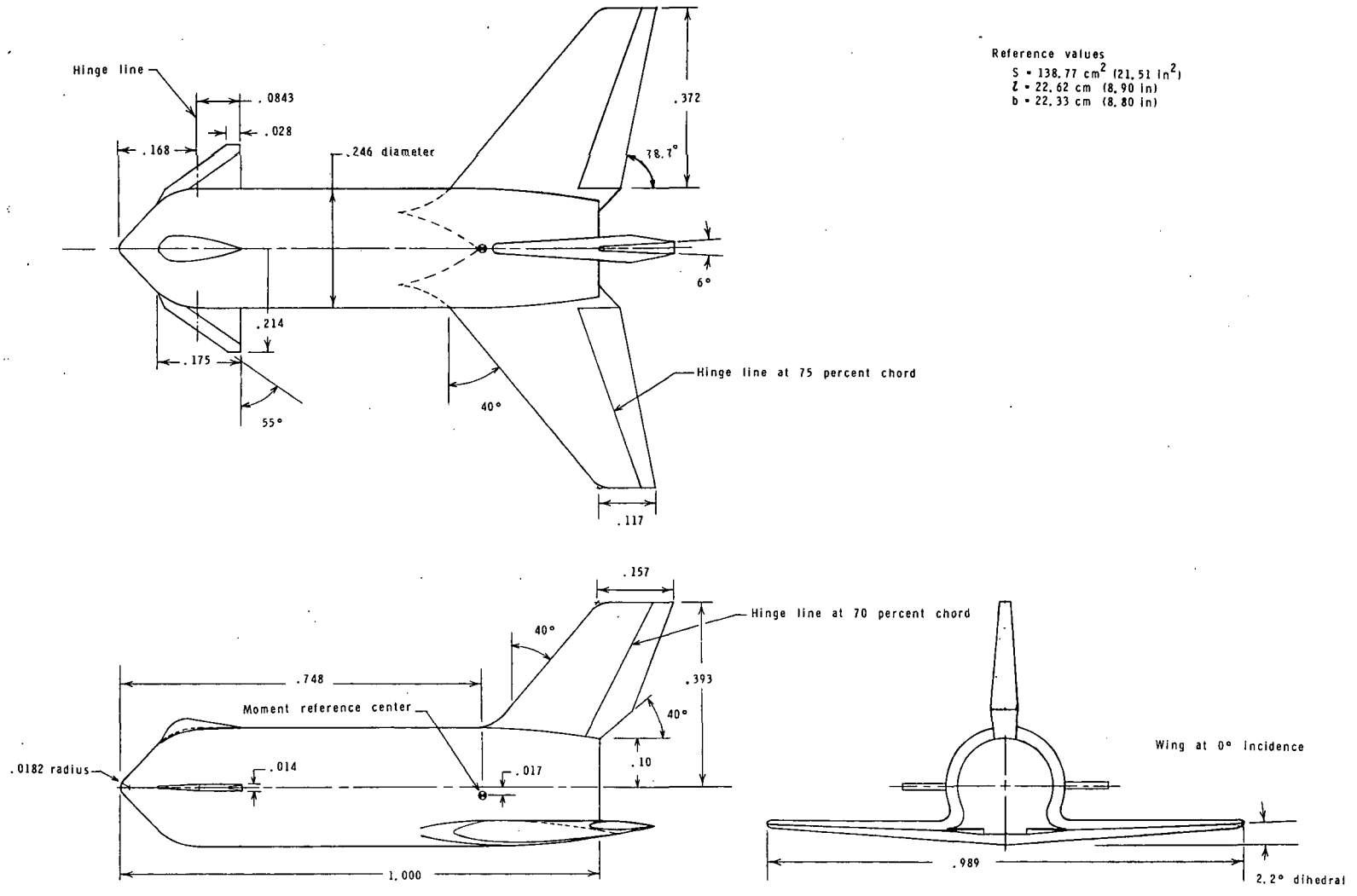

Figure 1.- Booster model. All dimensions are normalized with respect to fuselage length ℓ.

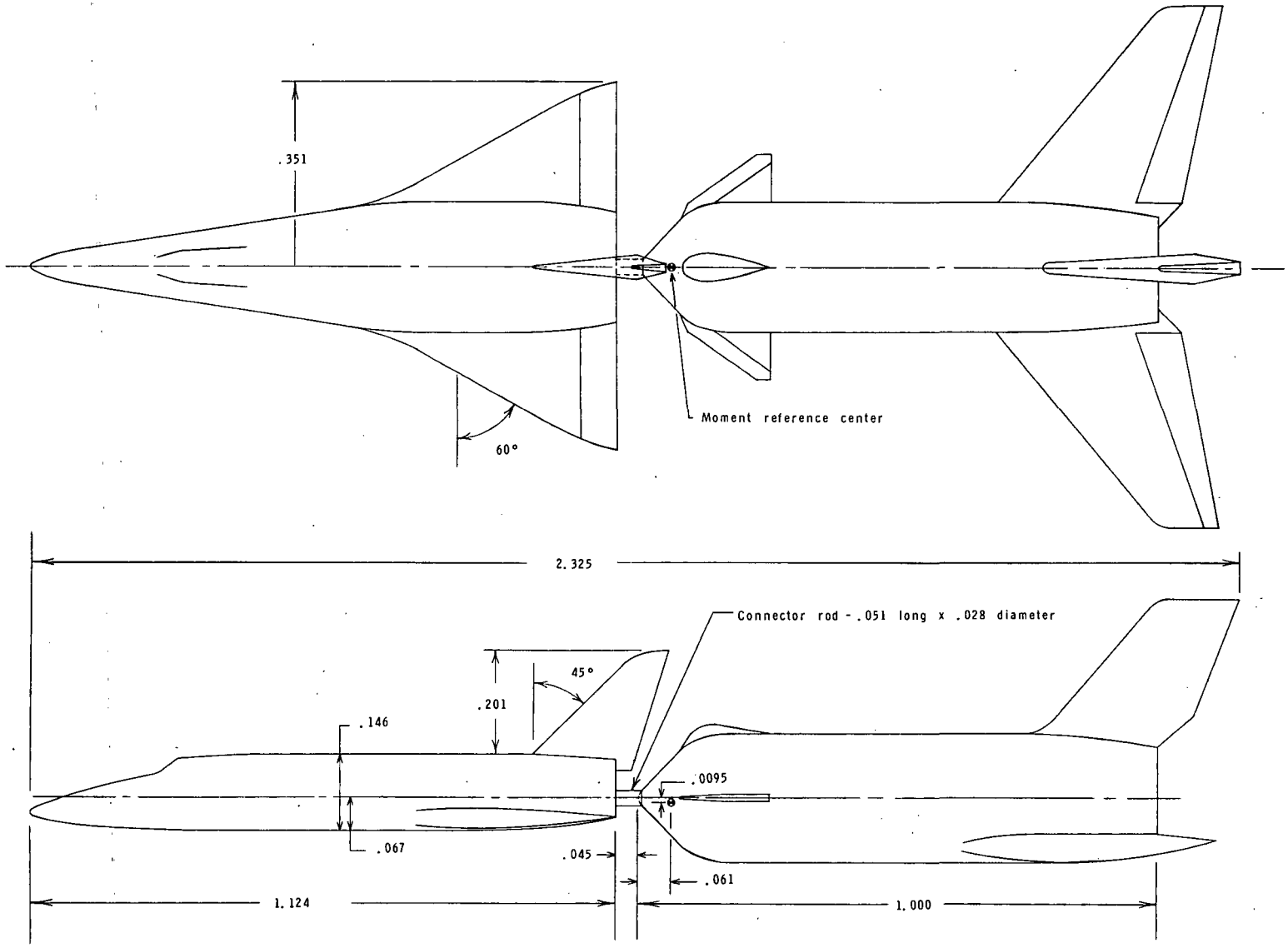

Figure 2.- Ascent configuration. All dimensions are normalized with respect to booster fuselage length l.

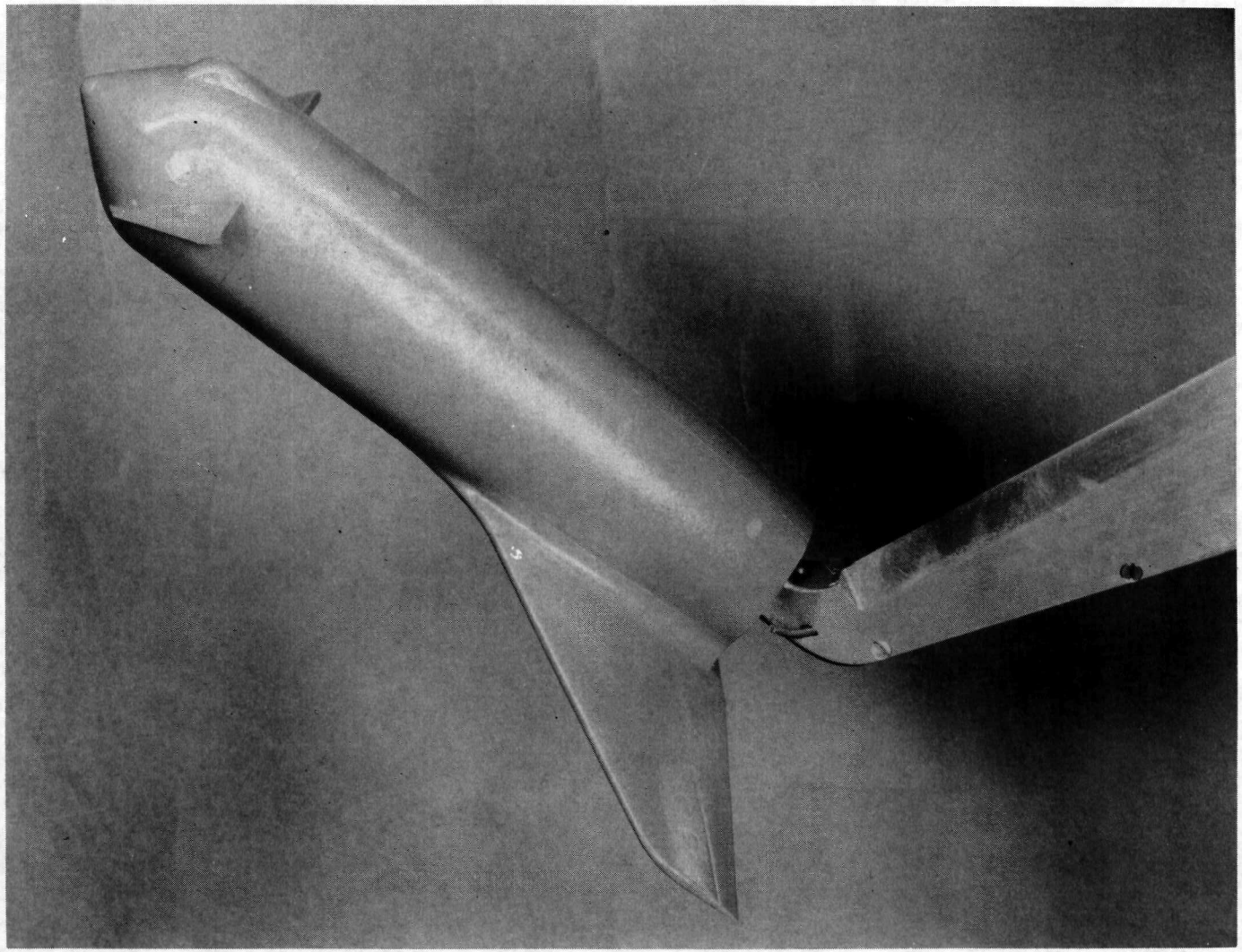

L-72-6531

(a) Configuration BCW; $\delta_e = 0^o$; $\delta_c = -60^o$.

Figure 3.- Photographs of several test configurations.

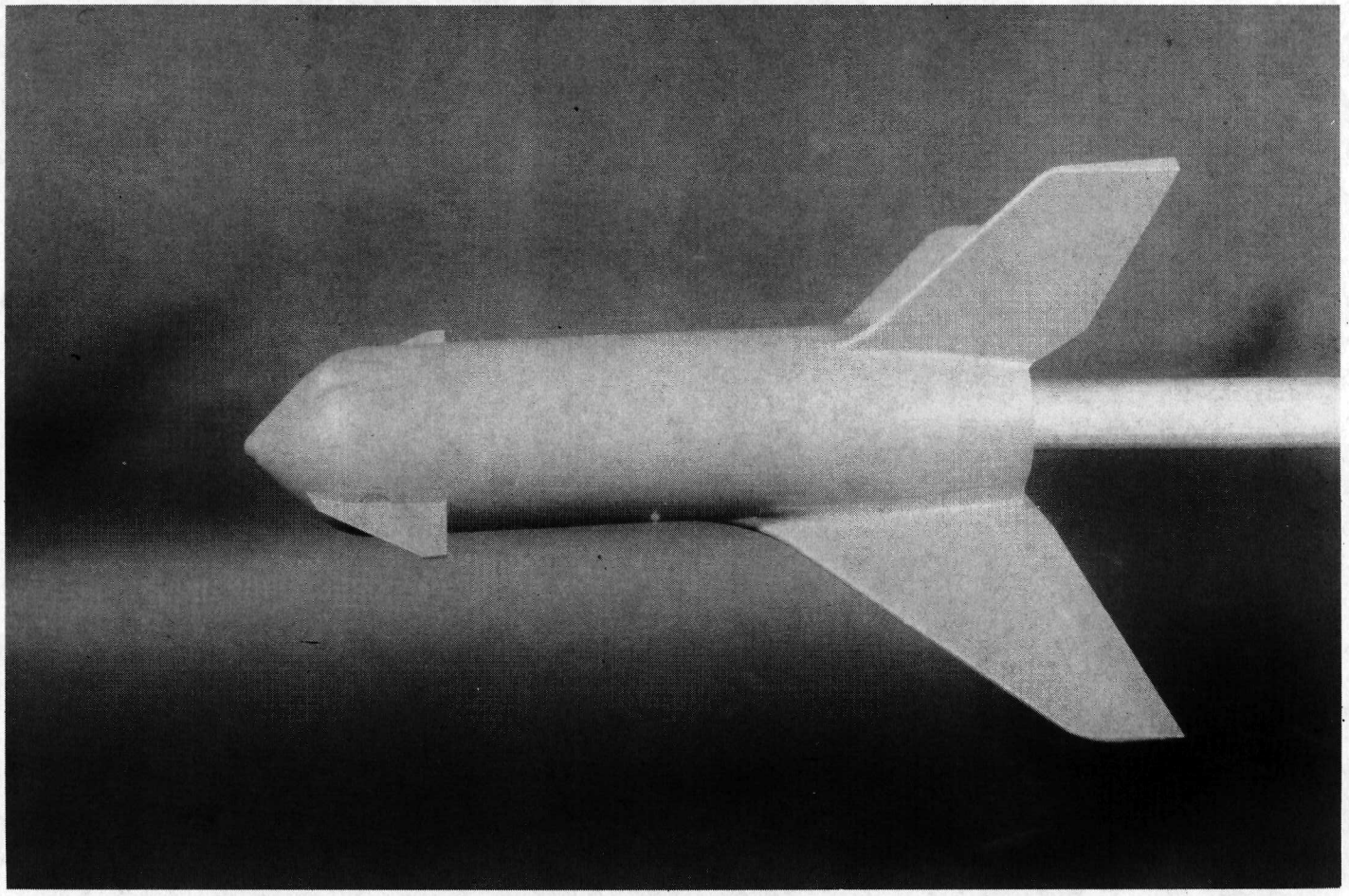

L-72-6532

(b) Configuration BCWV; $\delta_e = \delta_c = 0^o$.

Figure 3.- Continued.

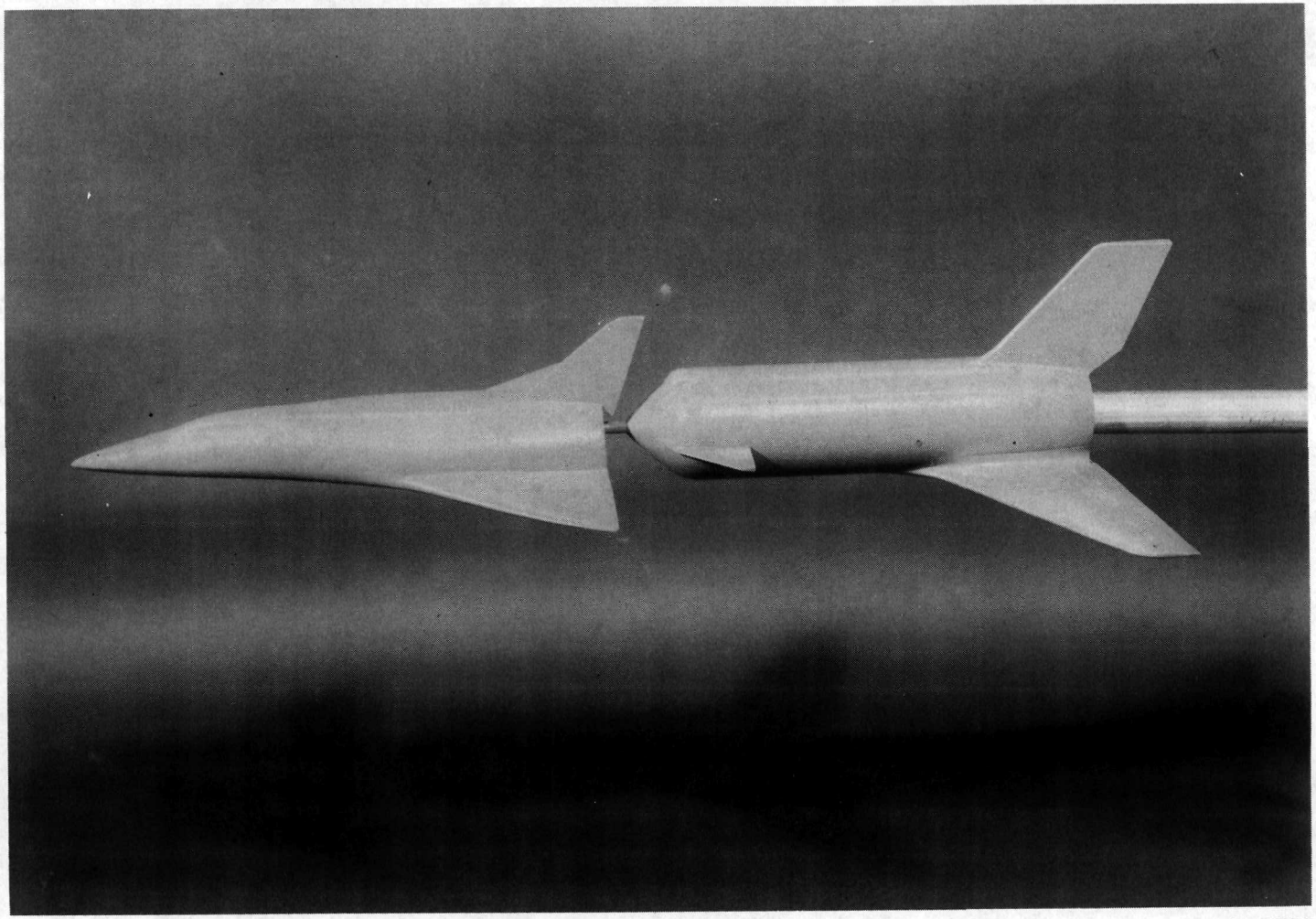

L-72-6533

(c) Ascent configuration.

Figure 3.- Concluded.

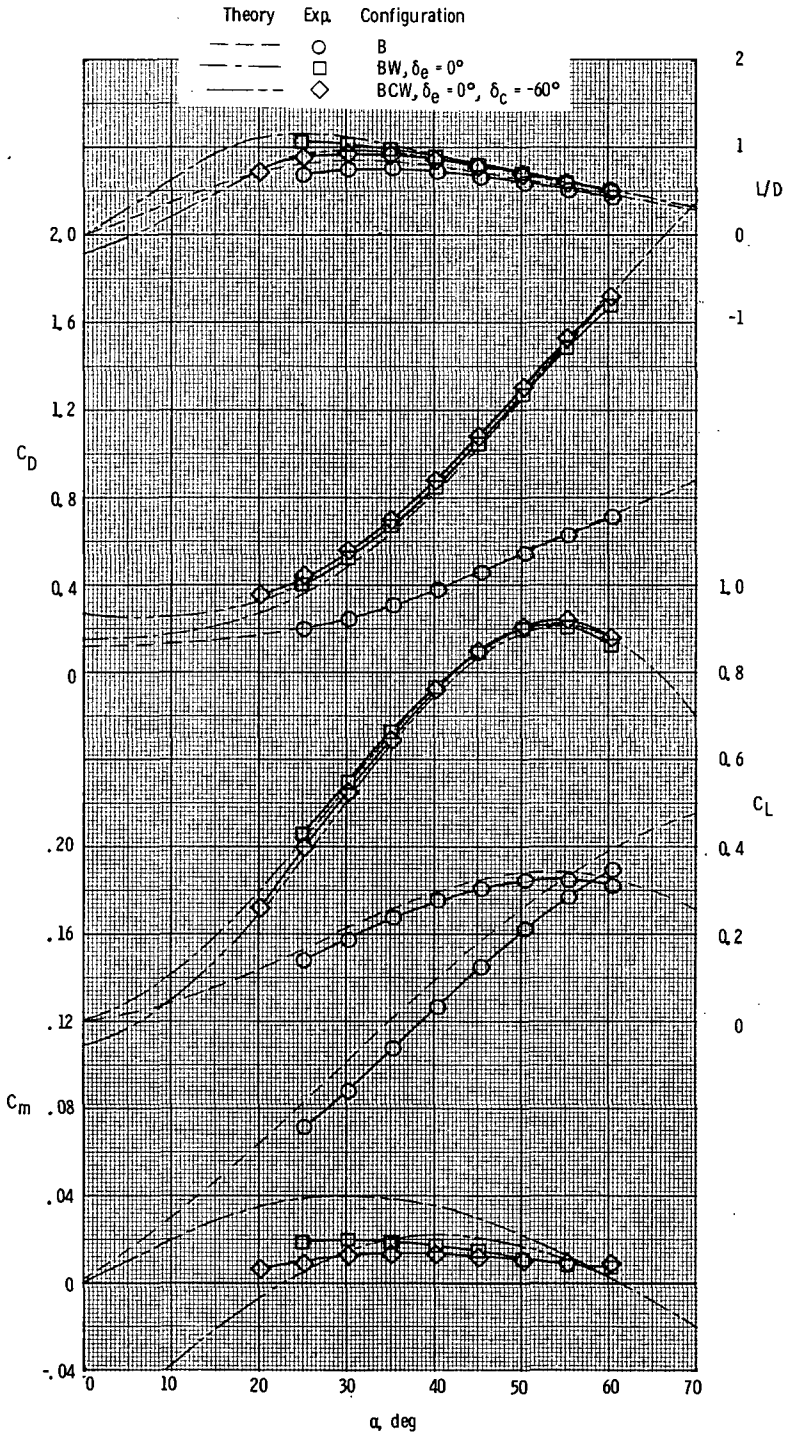

(a) Longitudinal characteristics (stability axis).

Figure 4.- Aerodynamic characteristics of booster components.

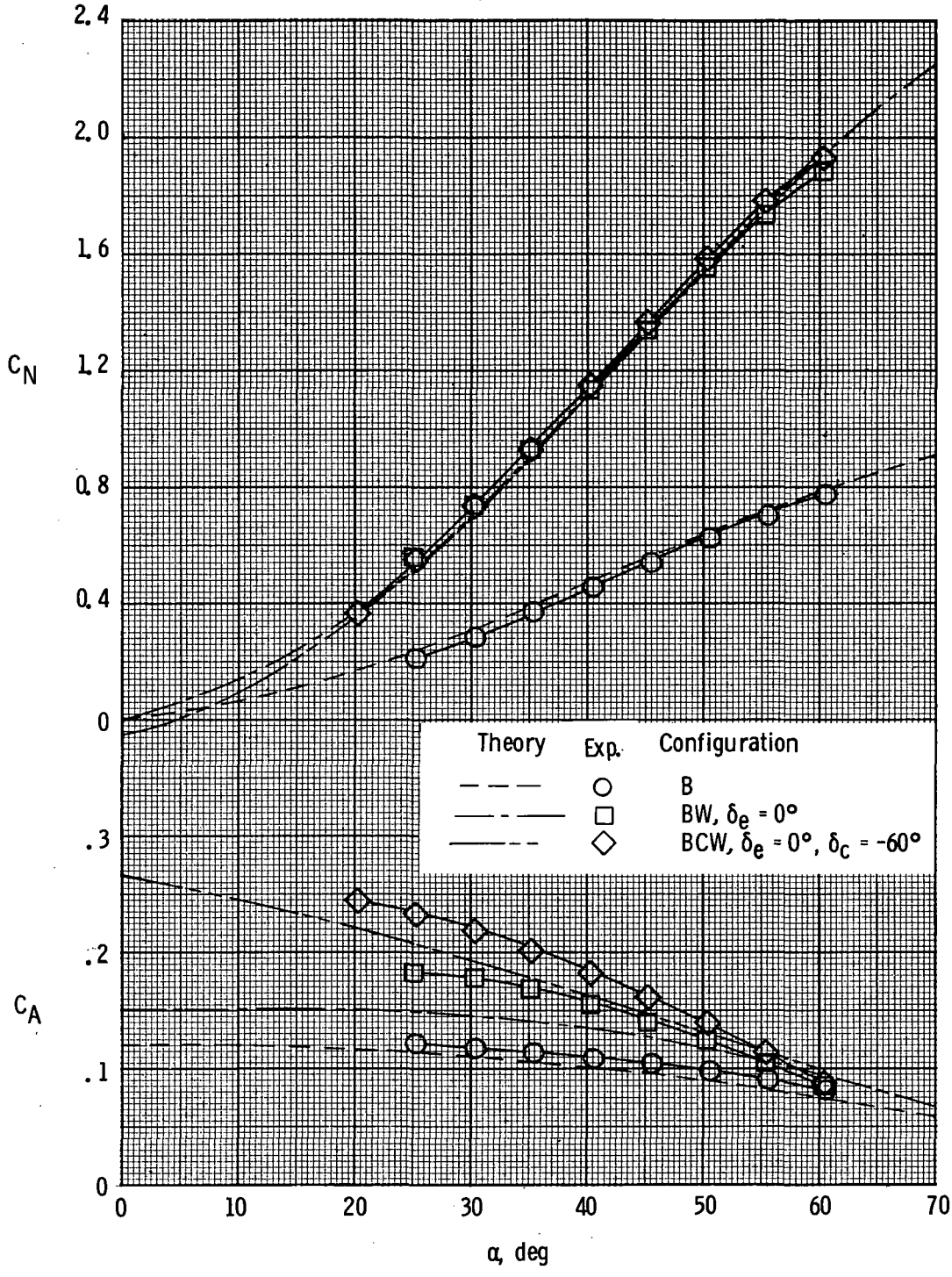

(b) Longitudinal characteristics (body axis).

Figure 4.- Continued.

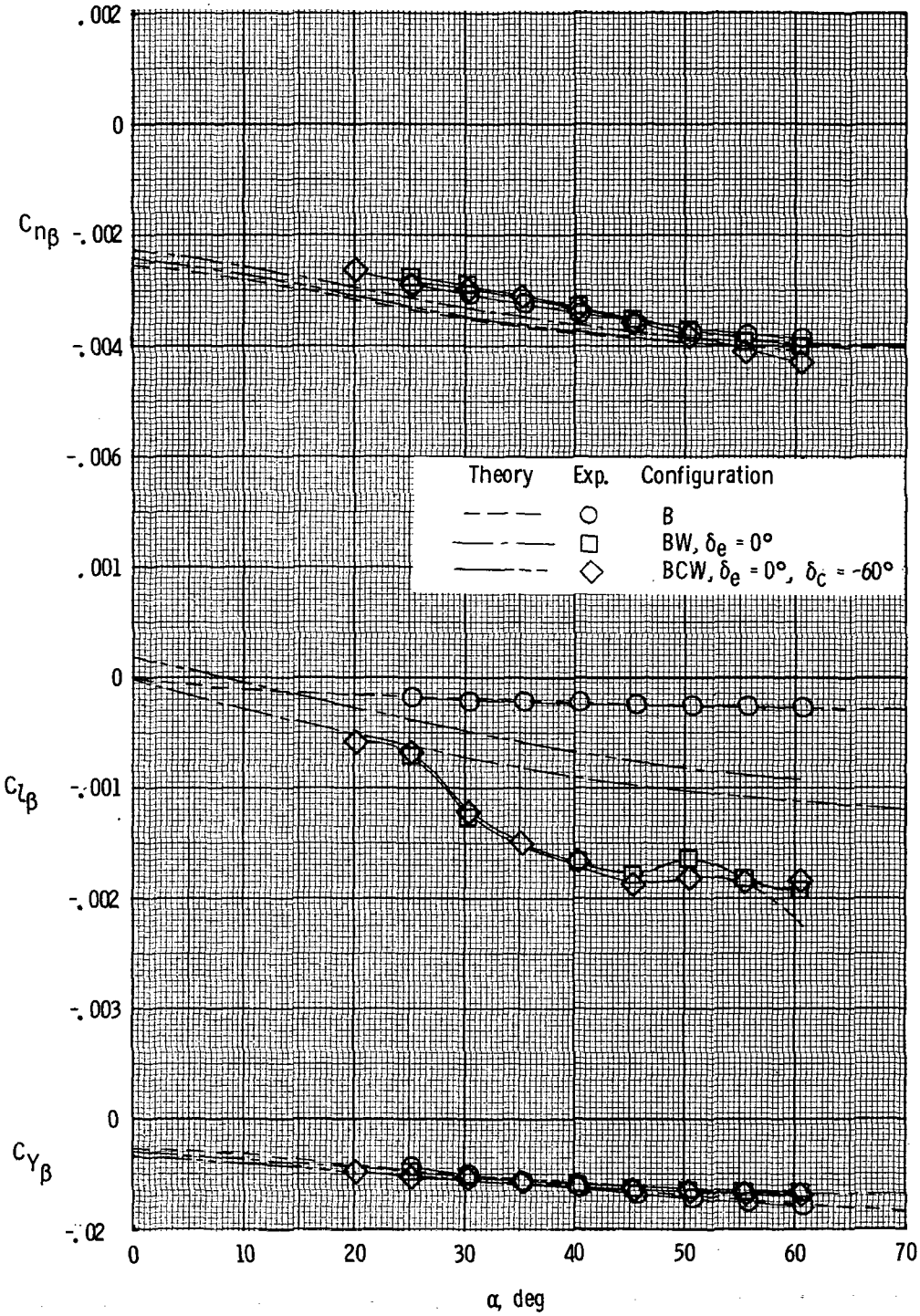

(c) Lateral-directional characteristics (body axis).

Figure 4.- Concluded.

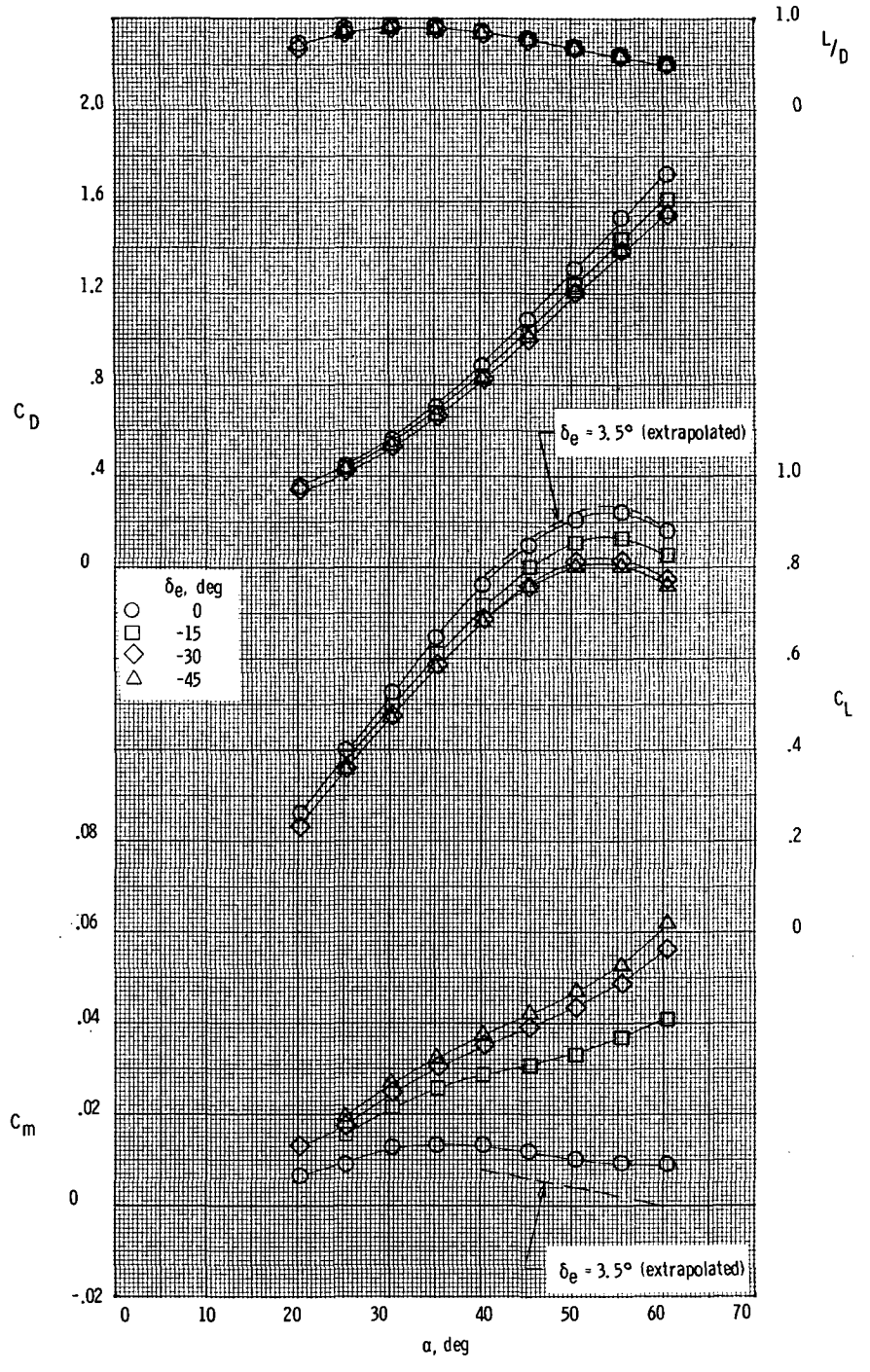

(a) Longitudinal characteristics (stability axis).

Figure 5.- Elevon effectiveness of configuration BCW. $\delta_c = -60^o$.

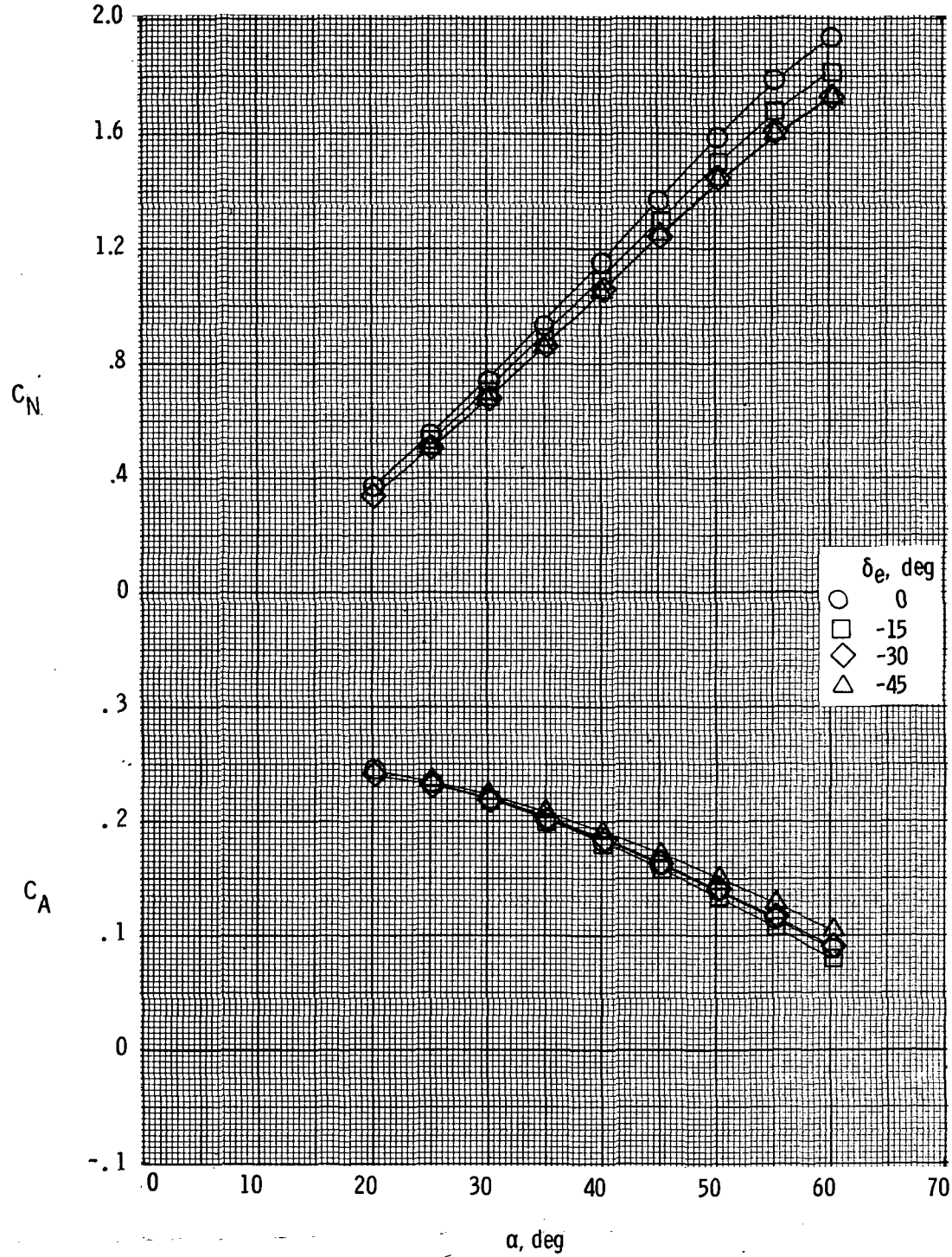

(b) Longitudinal characteristics (body axis).

Figure 5.- Continued.

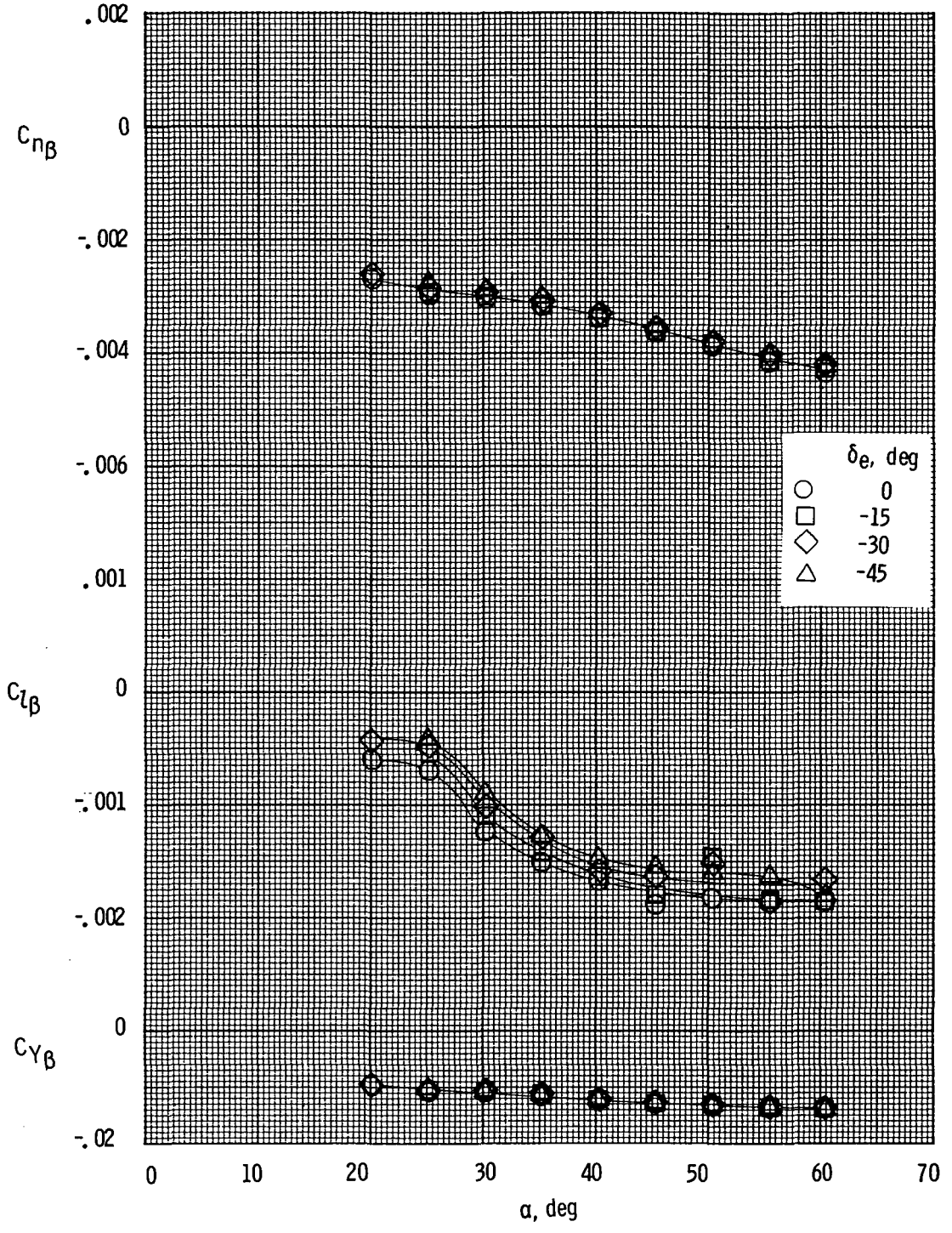

(c) Lateral-directional characteristics (body axis).

Figure 5.- Concluded.

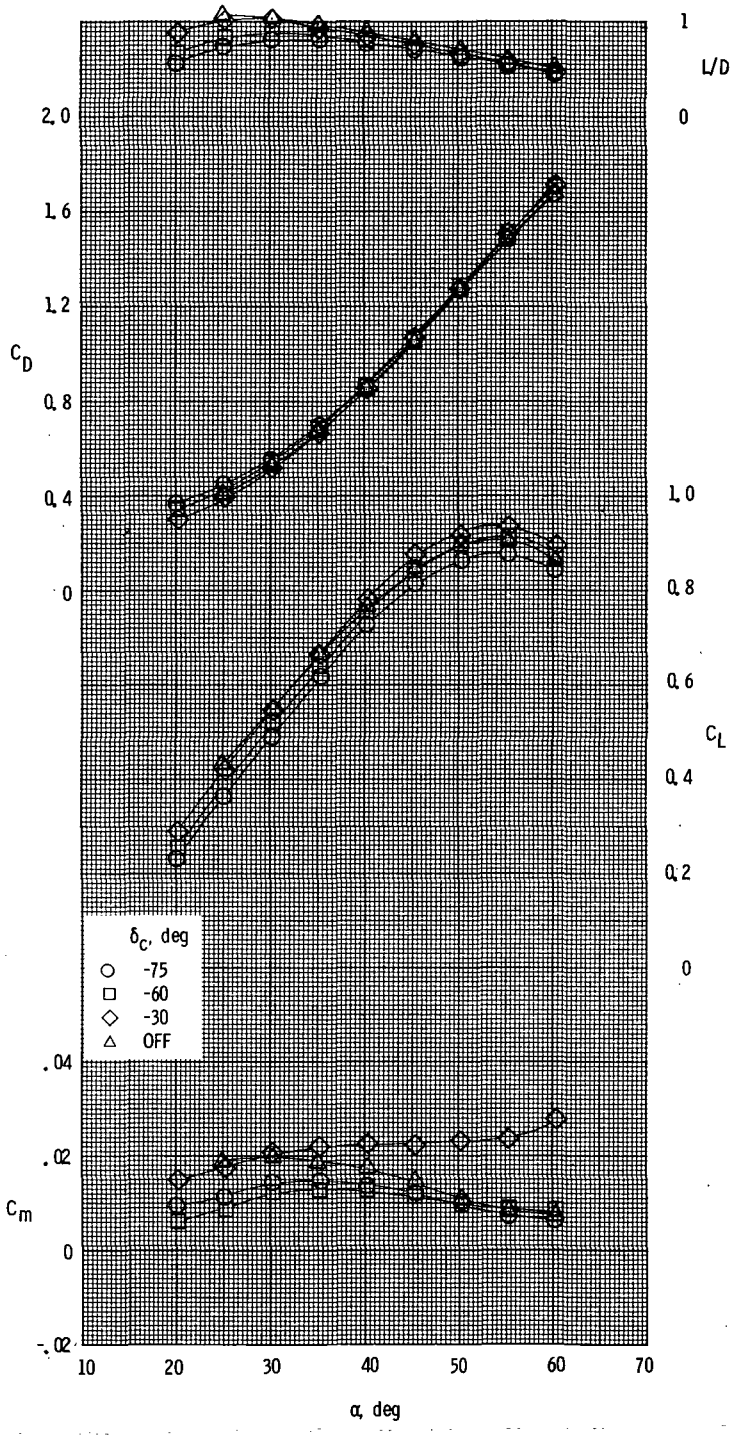

(a) Longitudinal characteristics (stability axis).

Figure 6.- Canard effectiveness of configuration BCW. $\delta_e = 0^o$.

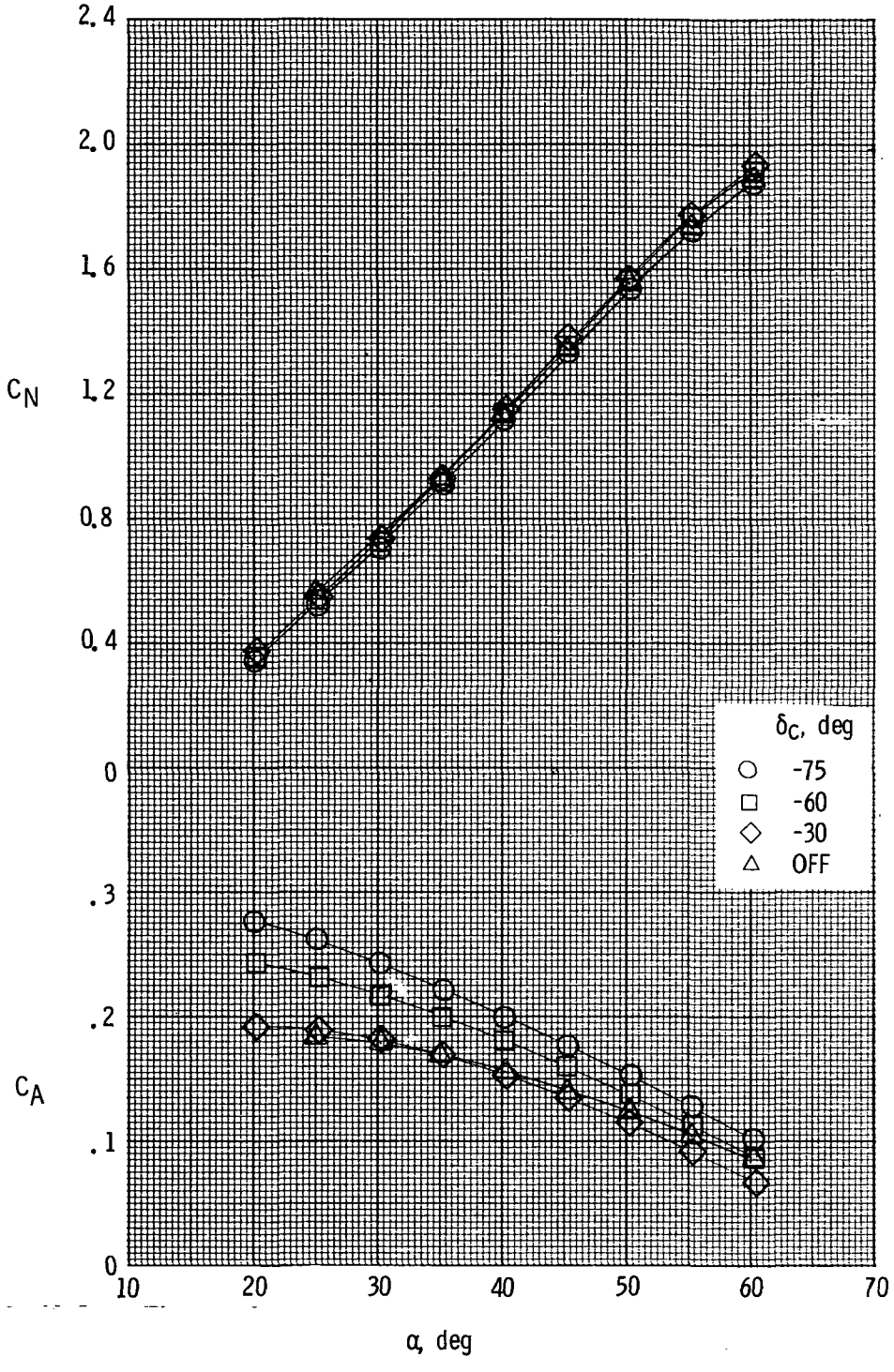

(b) Longitudinal characteristics (body axis).

Figure 6.- Continued.

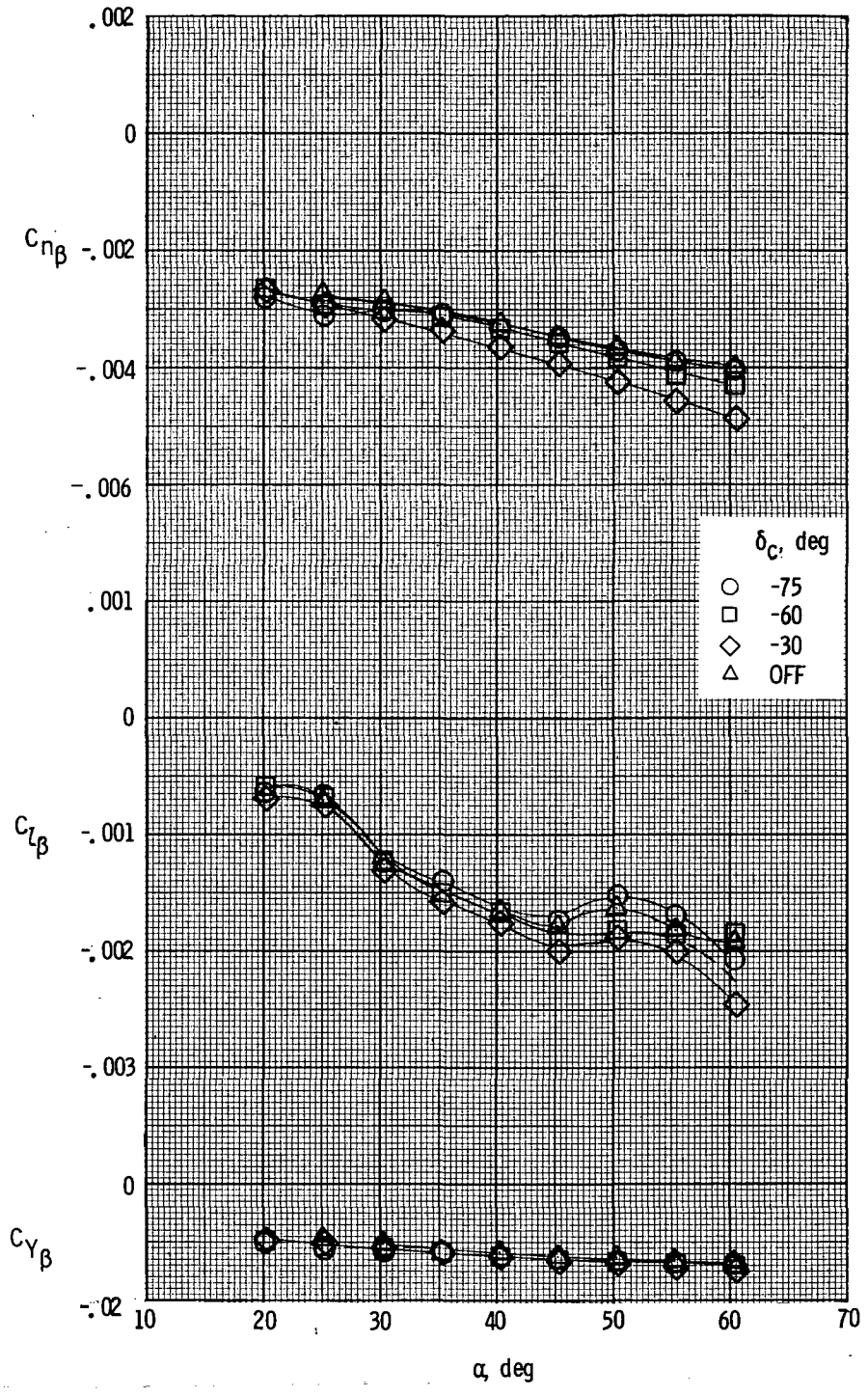

(c) Lateral-directional characteristics (body axis).

Figure 6.- Concluded.

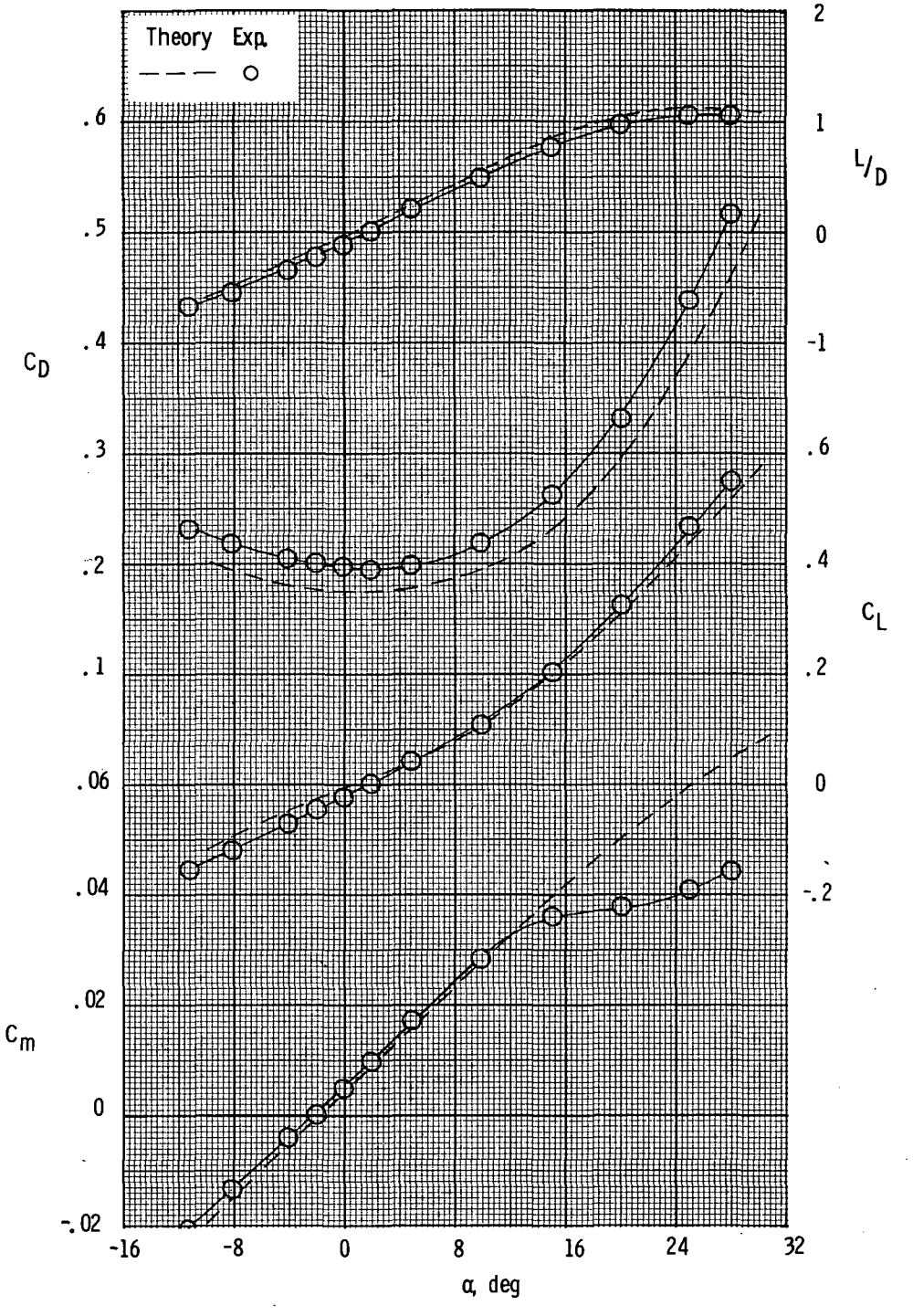

(a) Longitudinal characteristics (stability axis).

Figure 7.- Aerodynamic characteristics of configuration BCWV. $\delta_c = \delta_e = 0^o$.

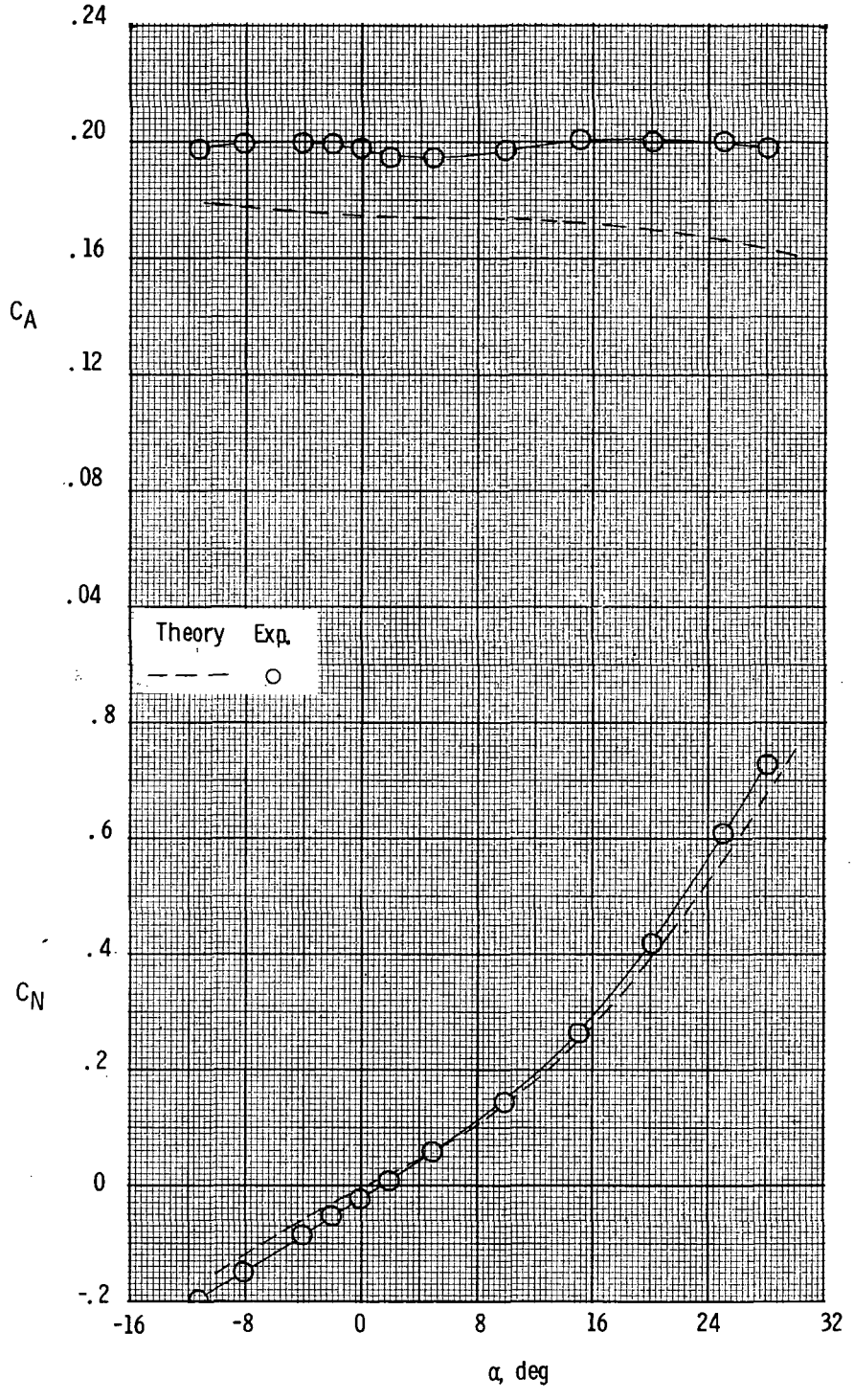

(b) Longitudinal characteristics (body axis).

Figure 7.- Continued.

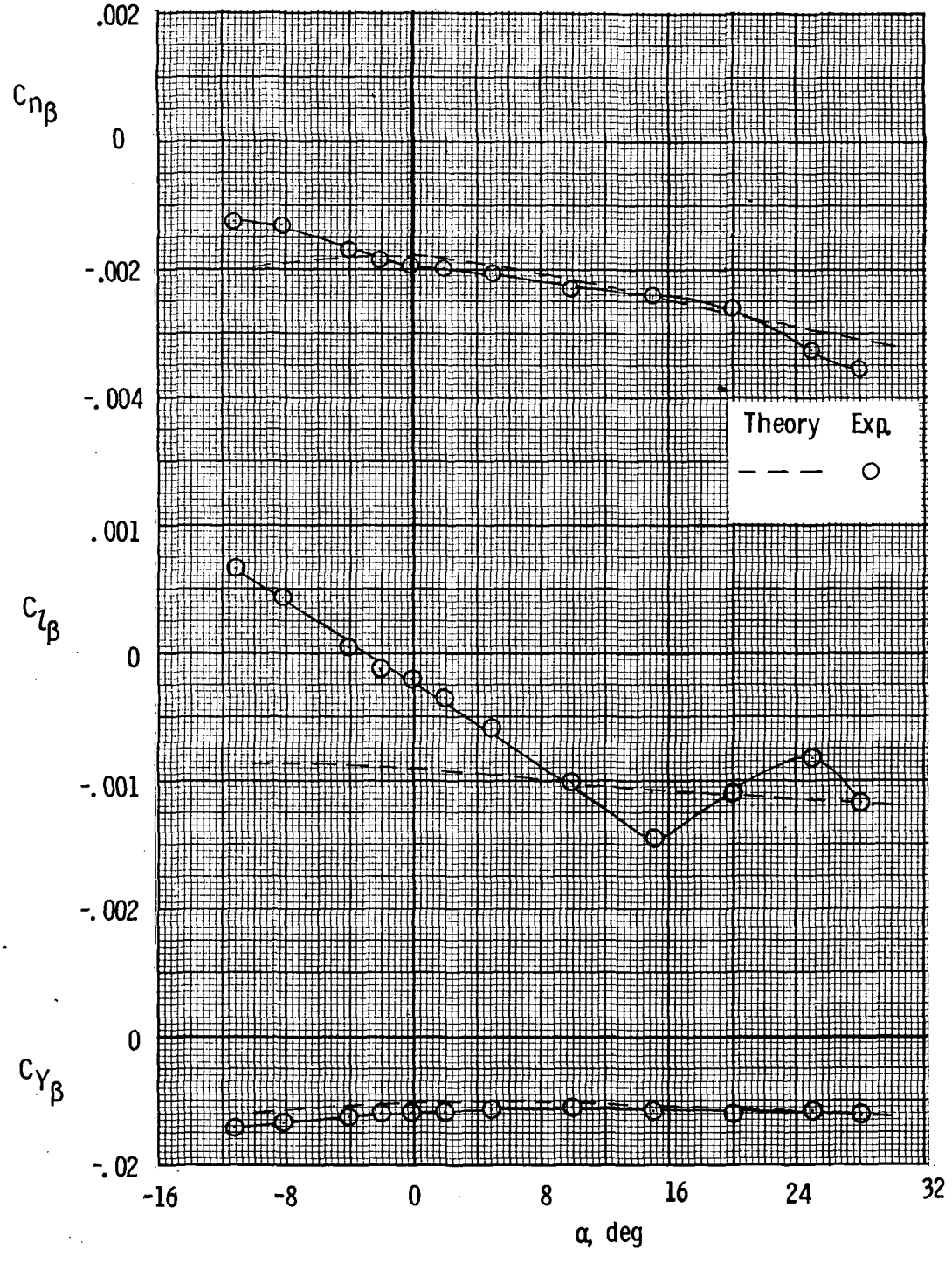

(c) Lateral-directional characteristics (body axis).

Figure 7.- Concluded.

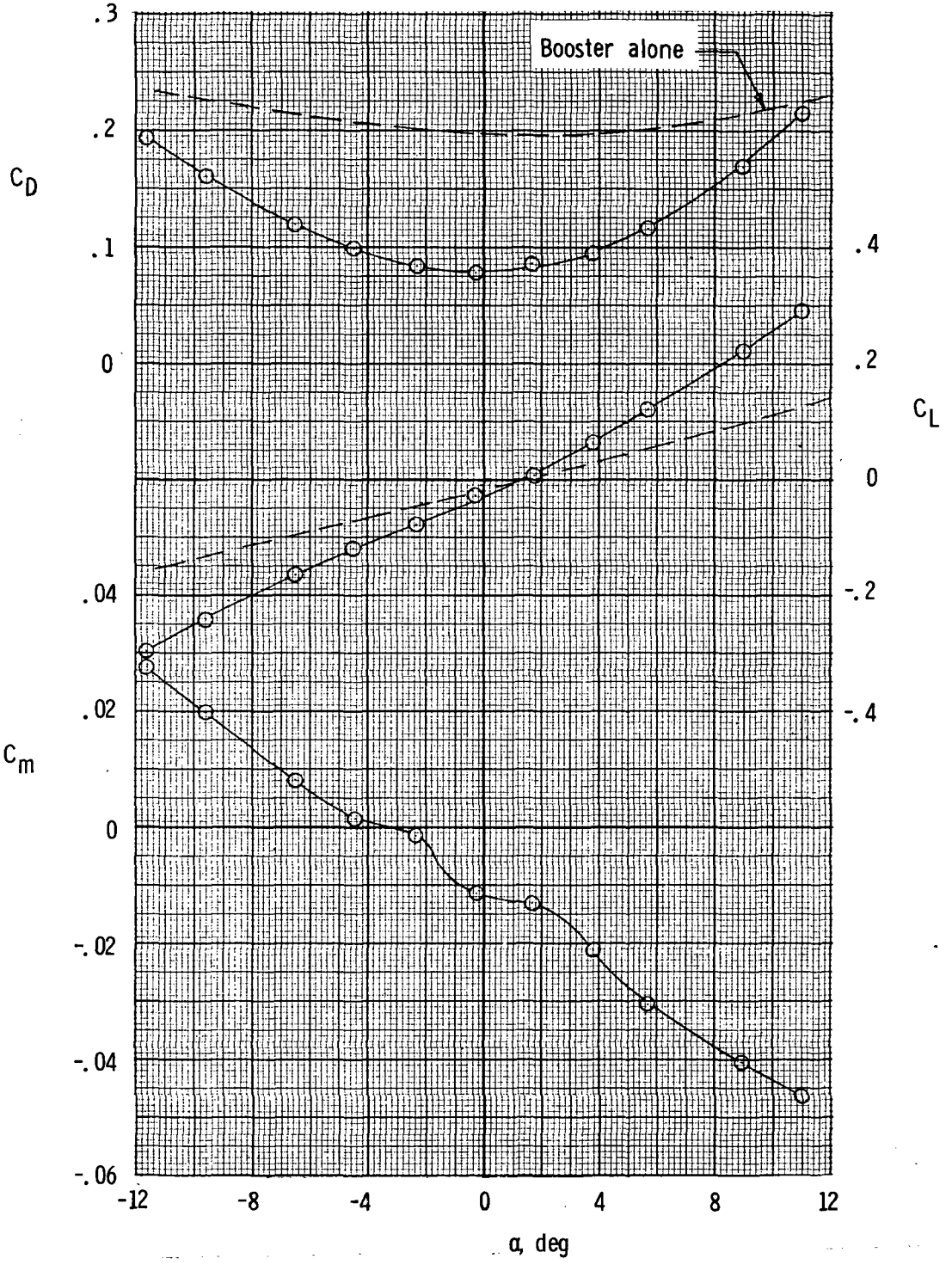

(a) Longitudinal characteristics (stability axis).

Figure 8.- Aerodynamic characteristics of ascent configuration.

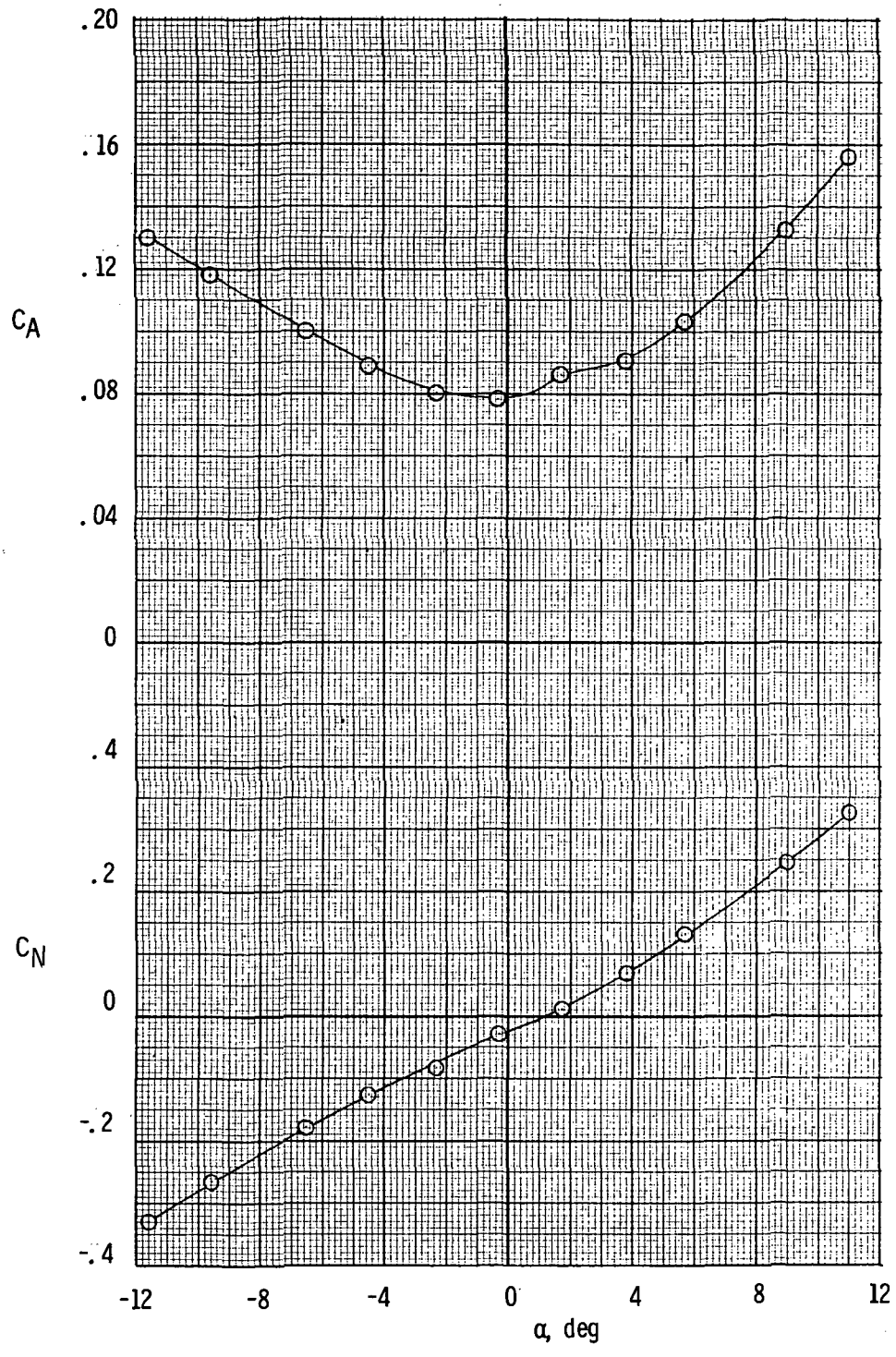

(b) Longitudinal characteristics (body axis).

Figure 8.- Continued.

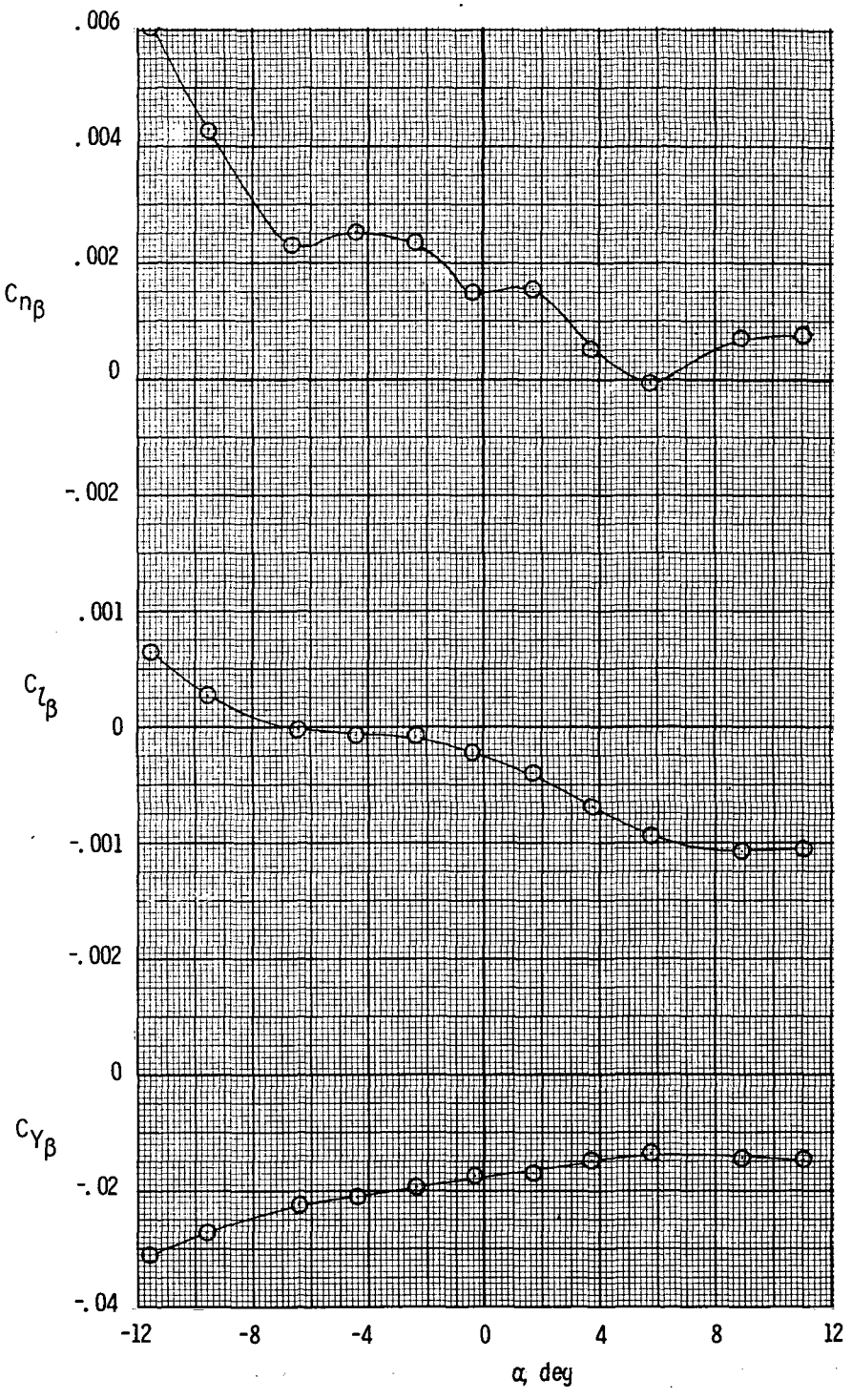

(c) Lateral-directional characteristics (body axis).

Figure 8.- Concluded.

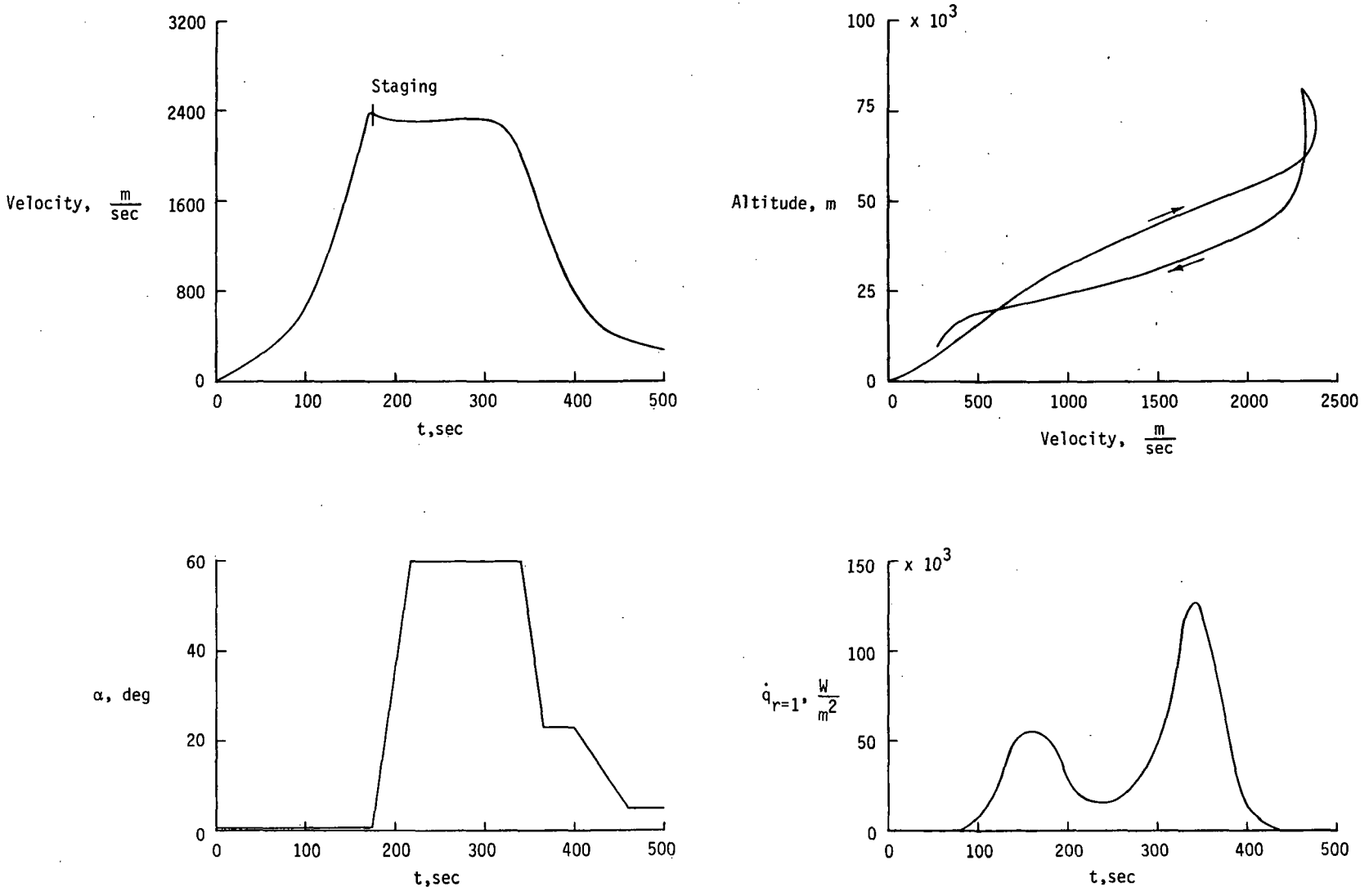

Figure 9.- Nominal ascent and return trajectory parameters.

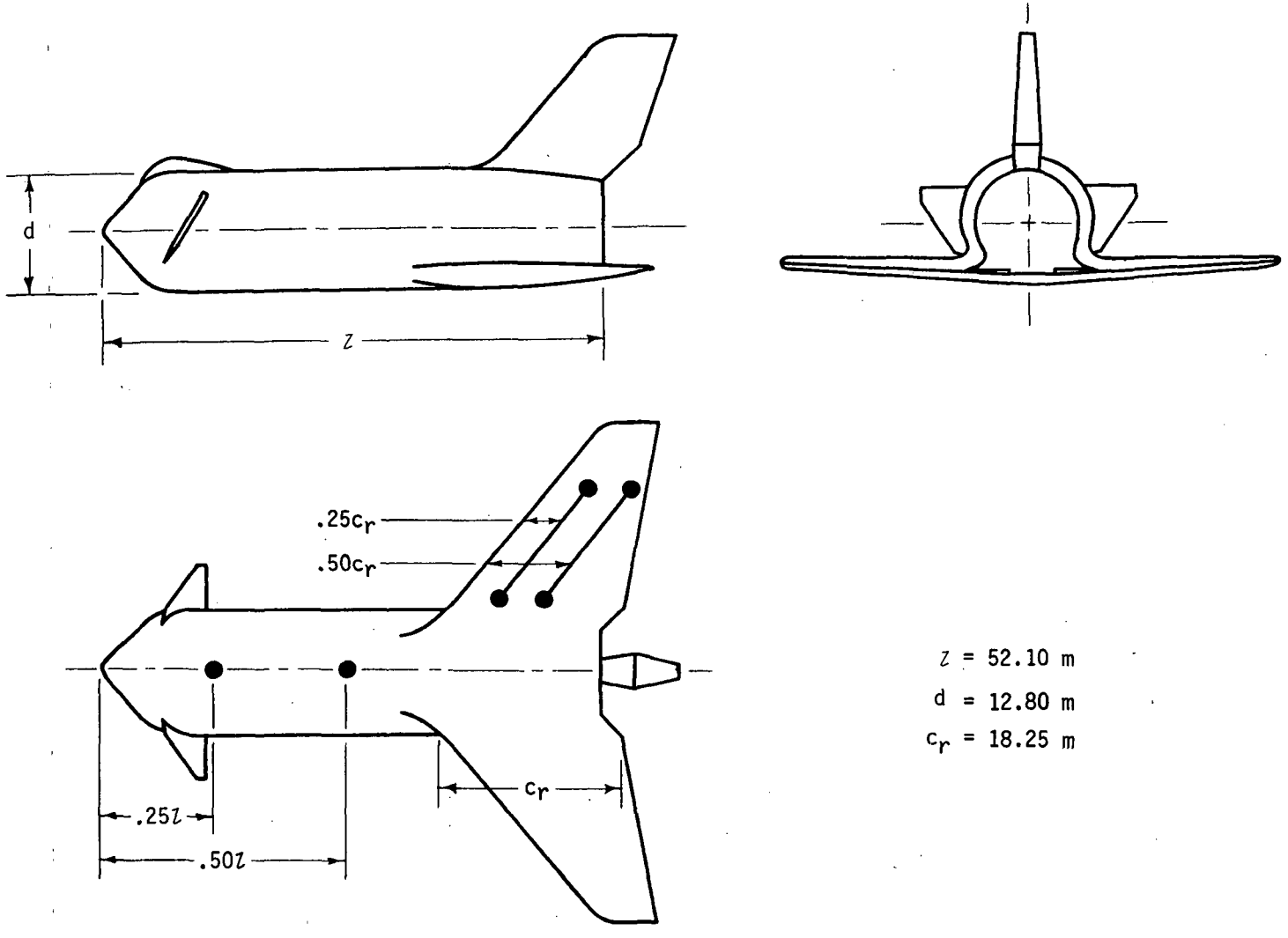

Figure 10.- Geometric location of computation reference points.

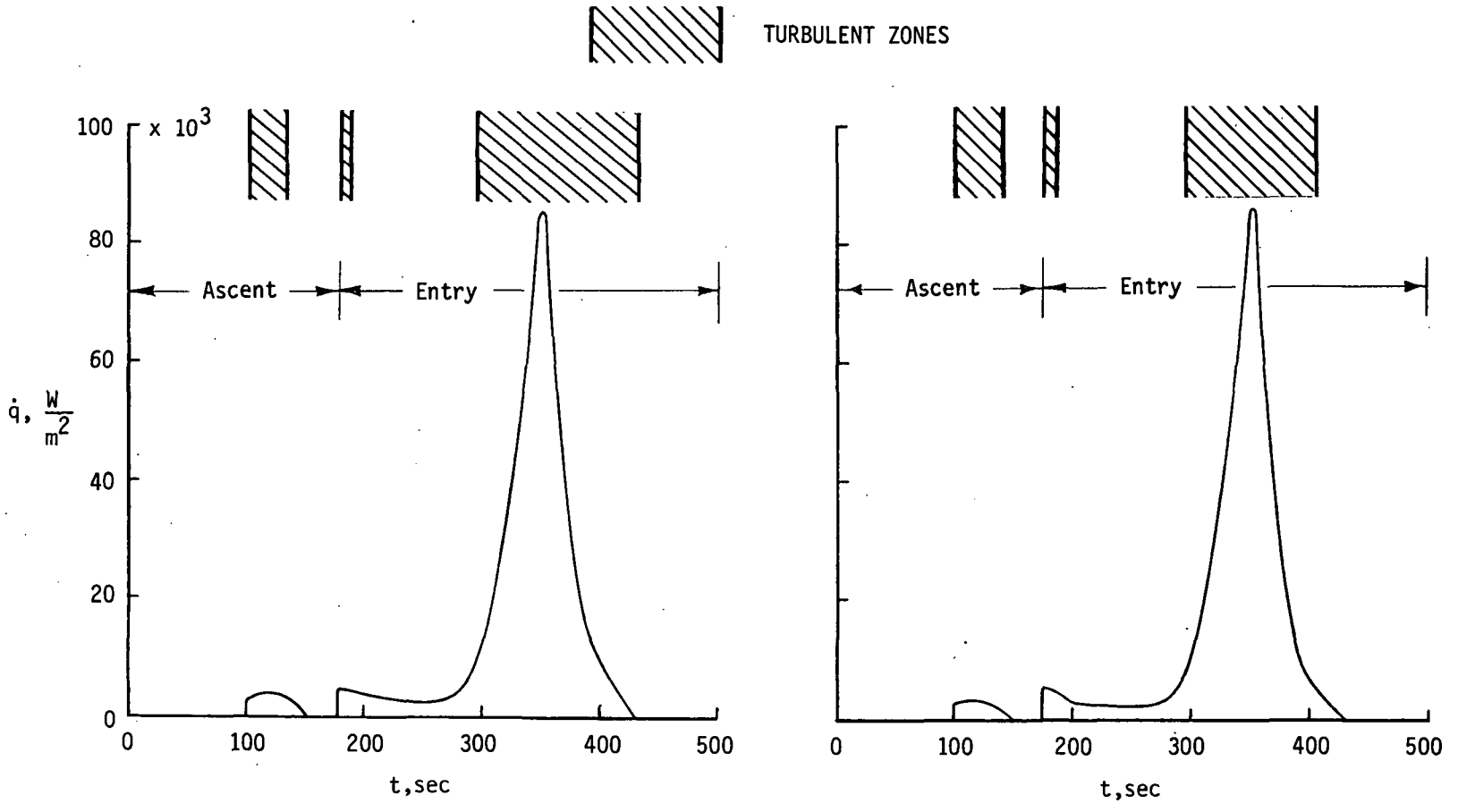

(a) $x/l = 0.25$.

(b) $x/l = 0.50$.

Figure 11.- Body reference-point heating-rate history (T = 311 K).

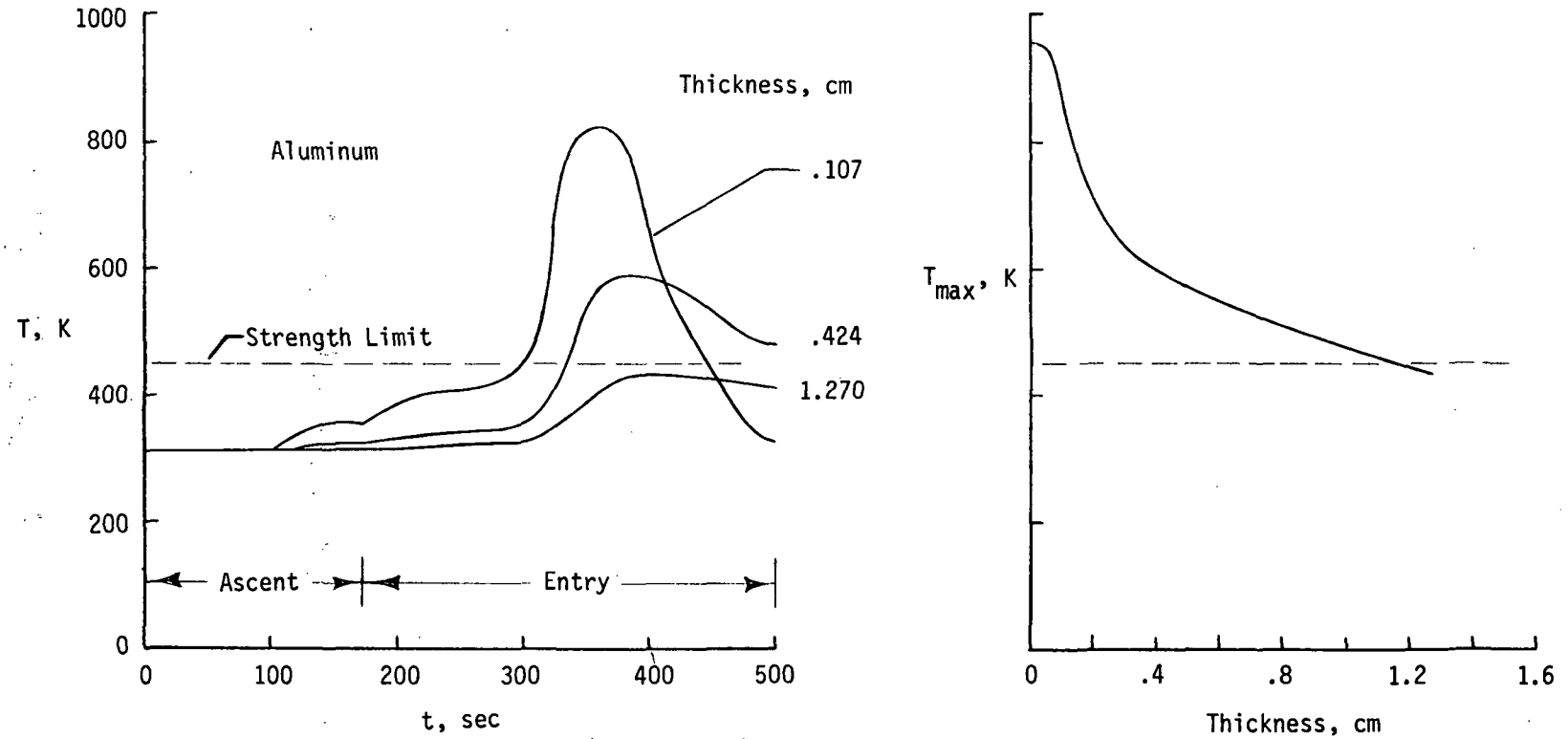

Figure 12.- Body reference-point skin-temperature history ($x/l = 0.25$).

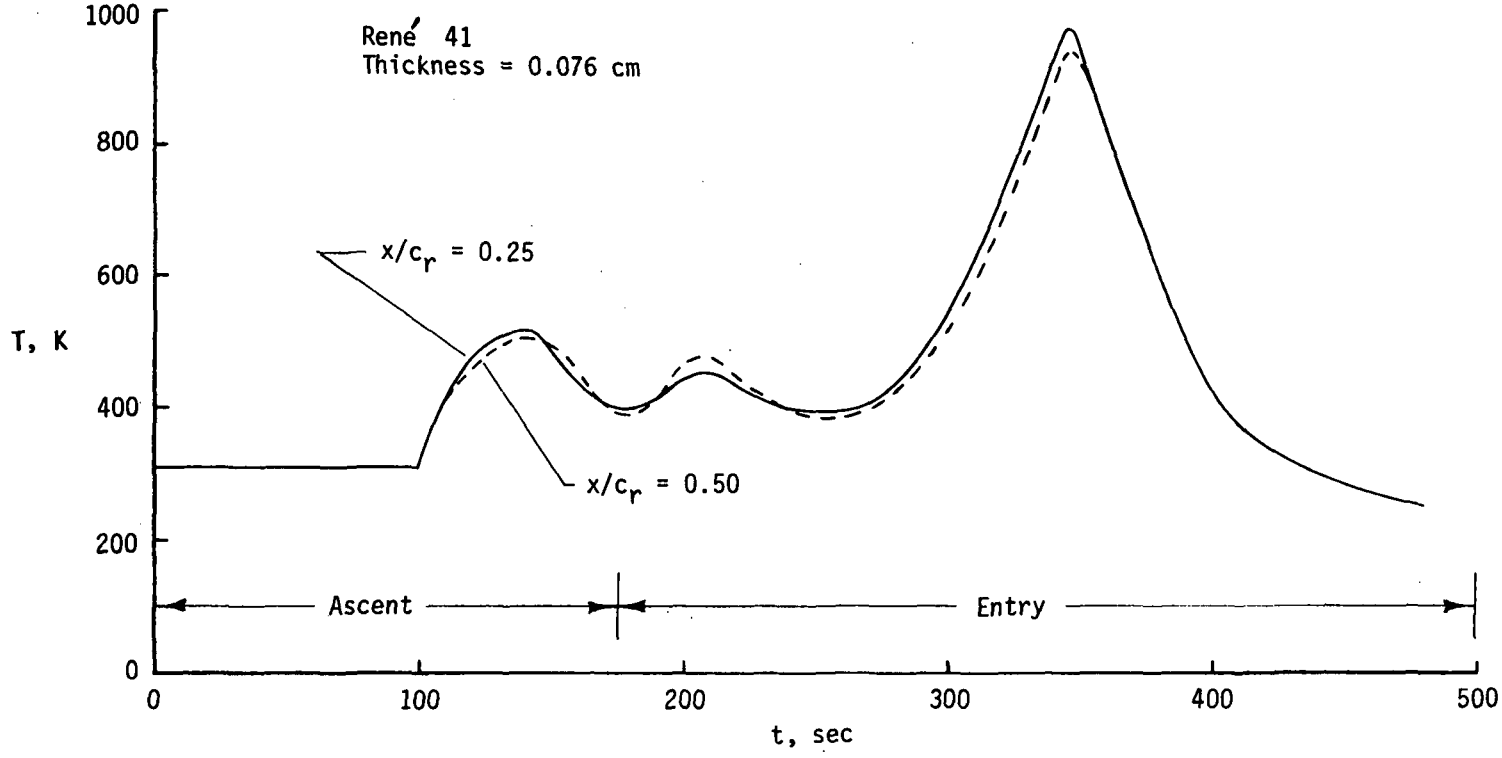

Figure 13.- Wing reference-point skin-temperature history.

Isotherm	h/h_{ref}
1	0.0904
2	0.0399
3	0.0221
4	0.0122

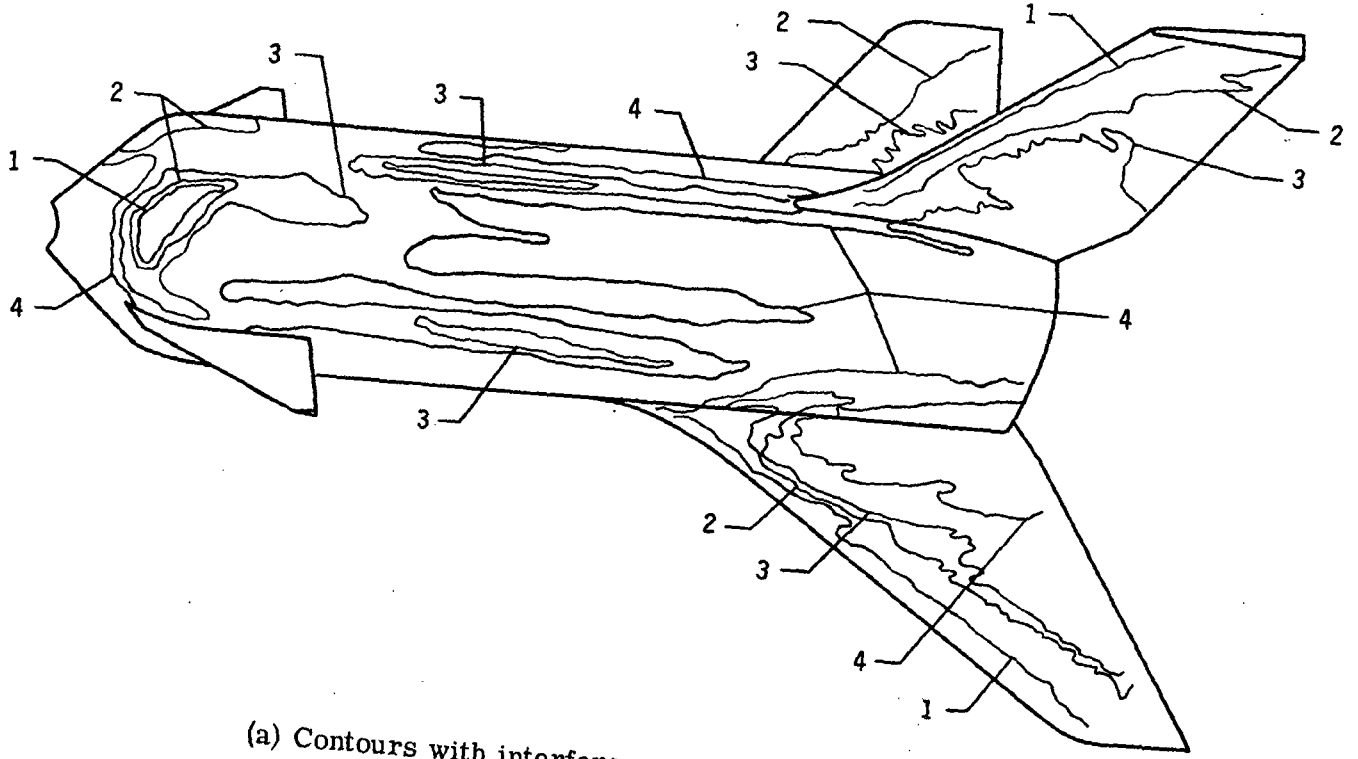

(a) Contours with interference on upper surface.

Figure 14.- Booster experimental heat-transfer contours. $M_\infty = 10.2$; $\alpha = 0^o$.

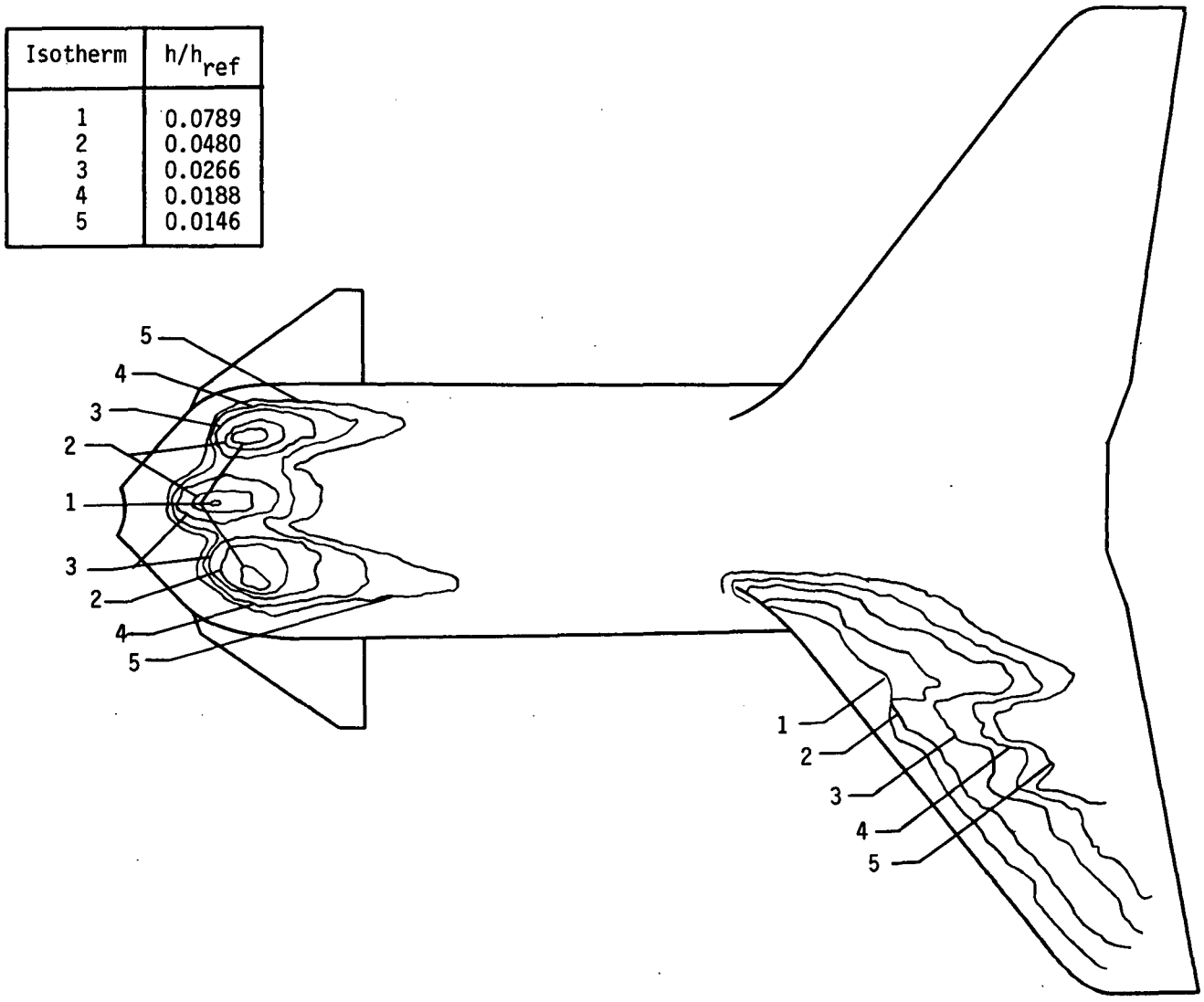

(b) Contours with interference on lower surface.

Figure 14.- Continued.

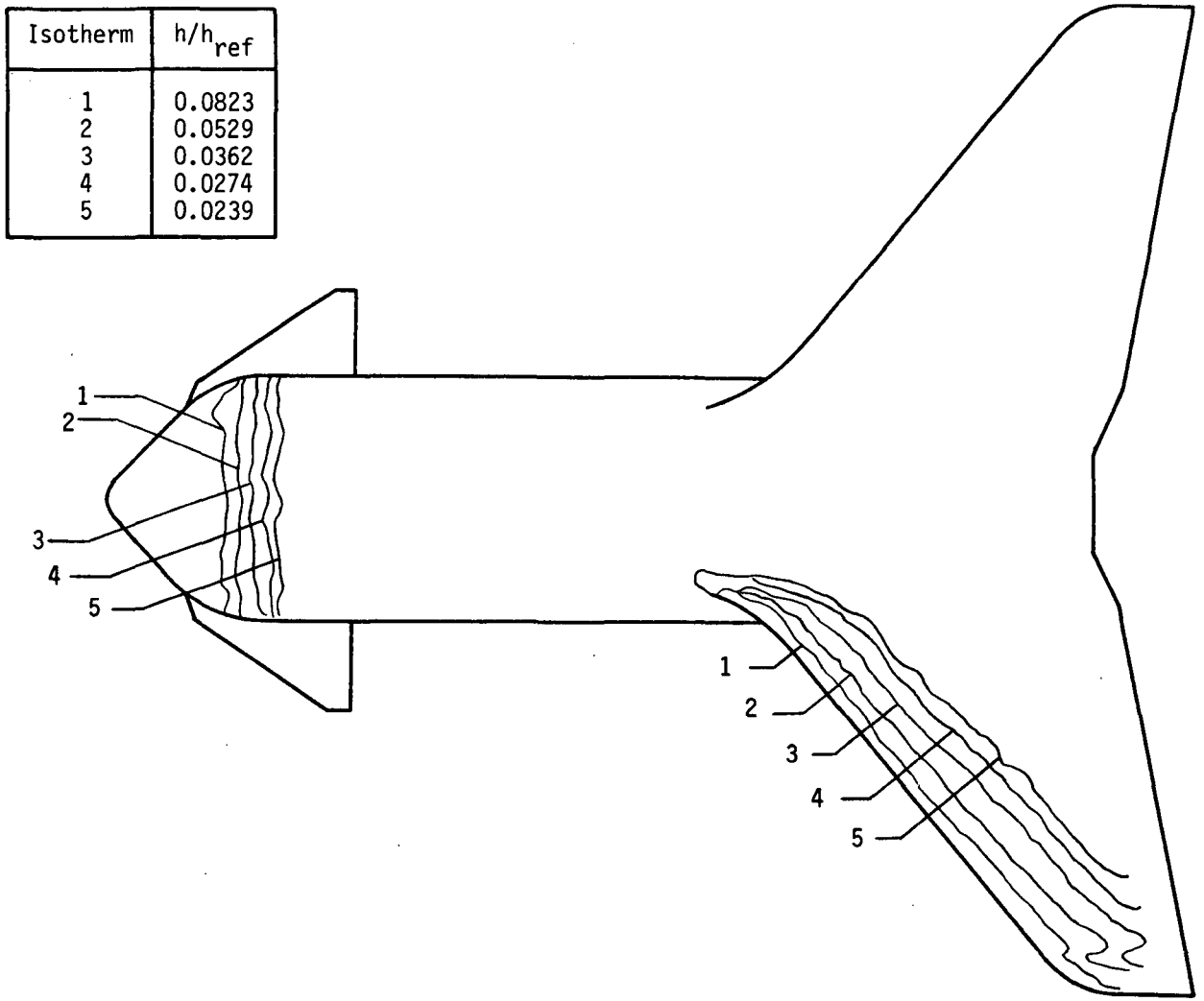

(c) Contours without interference on lower surface.

Figure 14.- Concluded.

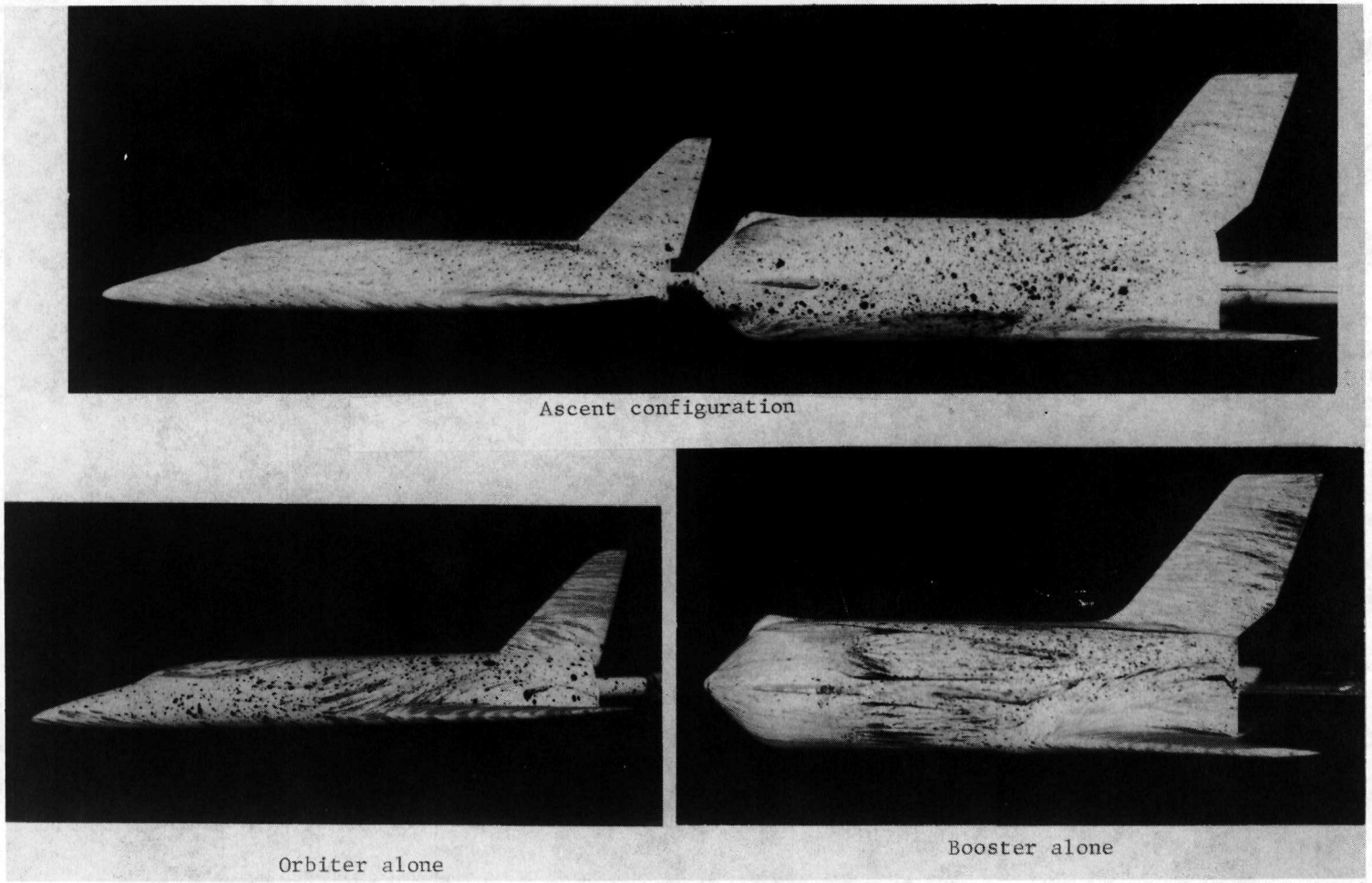

(a) Side view.

Figure 15.- Oil-flow photographs. $\delta_c = 0^o = \delta_e$; $\alpha = 0^o$.

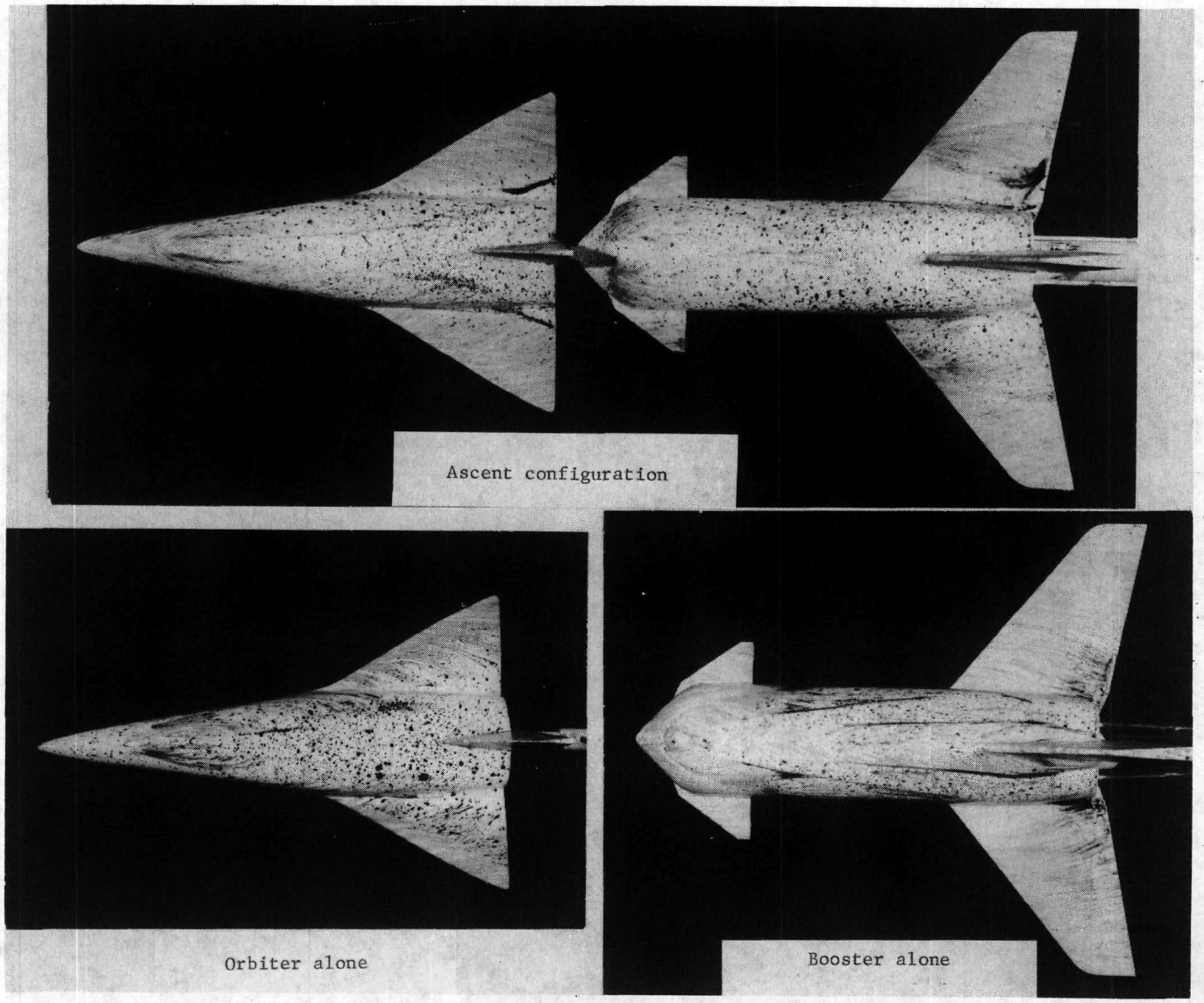

(b) Top view.

Figure 15.- Continued.

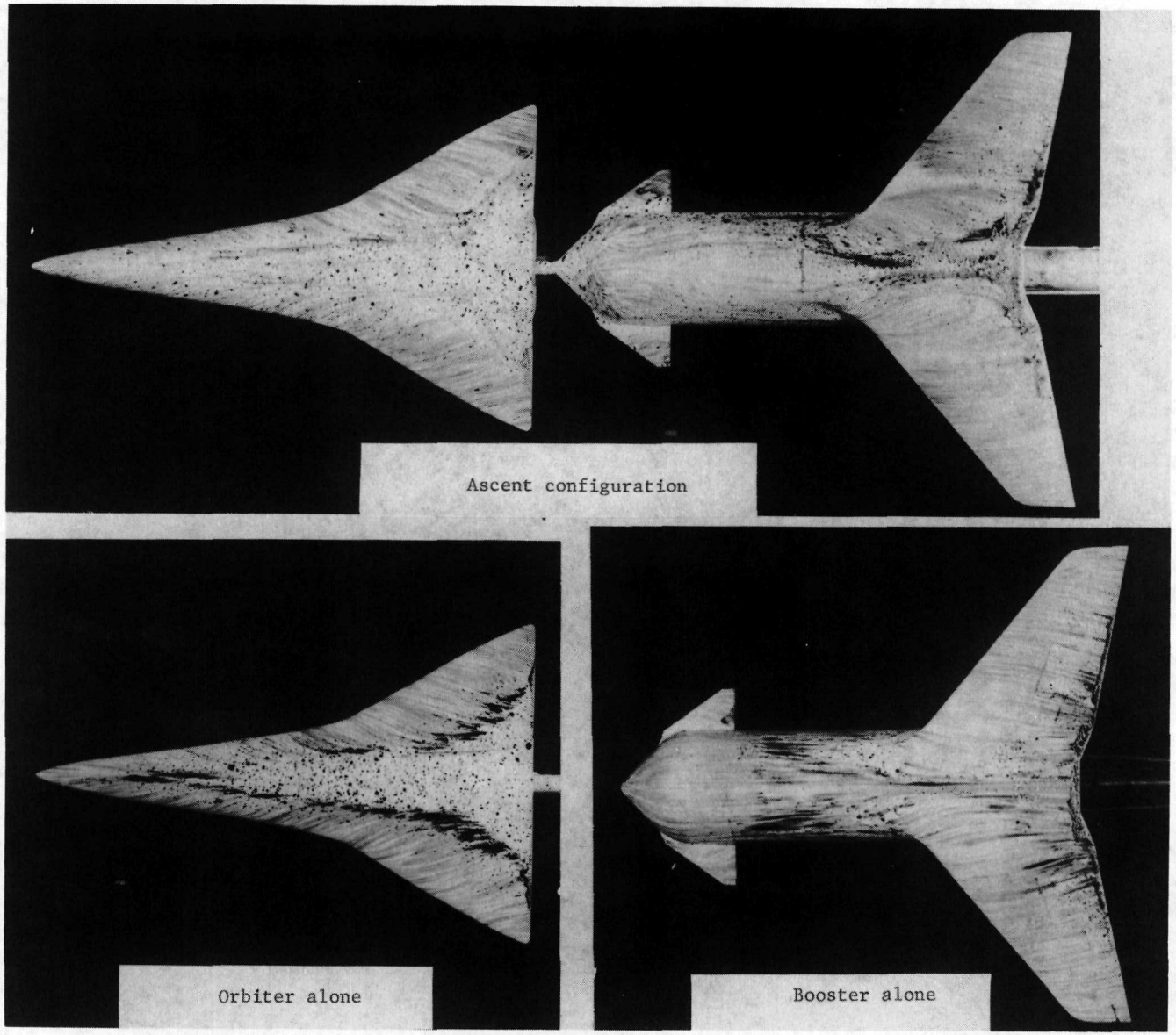

(c) Bottom view.

Figure 15.- Concluded.

L-72-6537

(a) Side view.

Figure 16.- Oil-flow photographs of configuration BCW.
$\alpha = 60^{o}$; $\delta_c = -60^{o}$; $\delta_e = 0^{o}$.

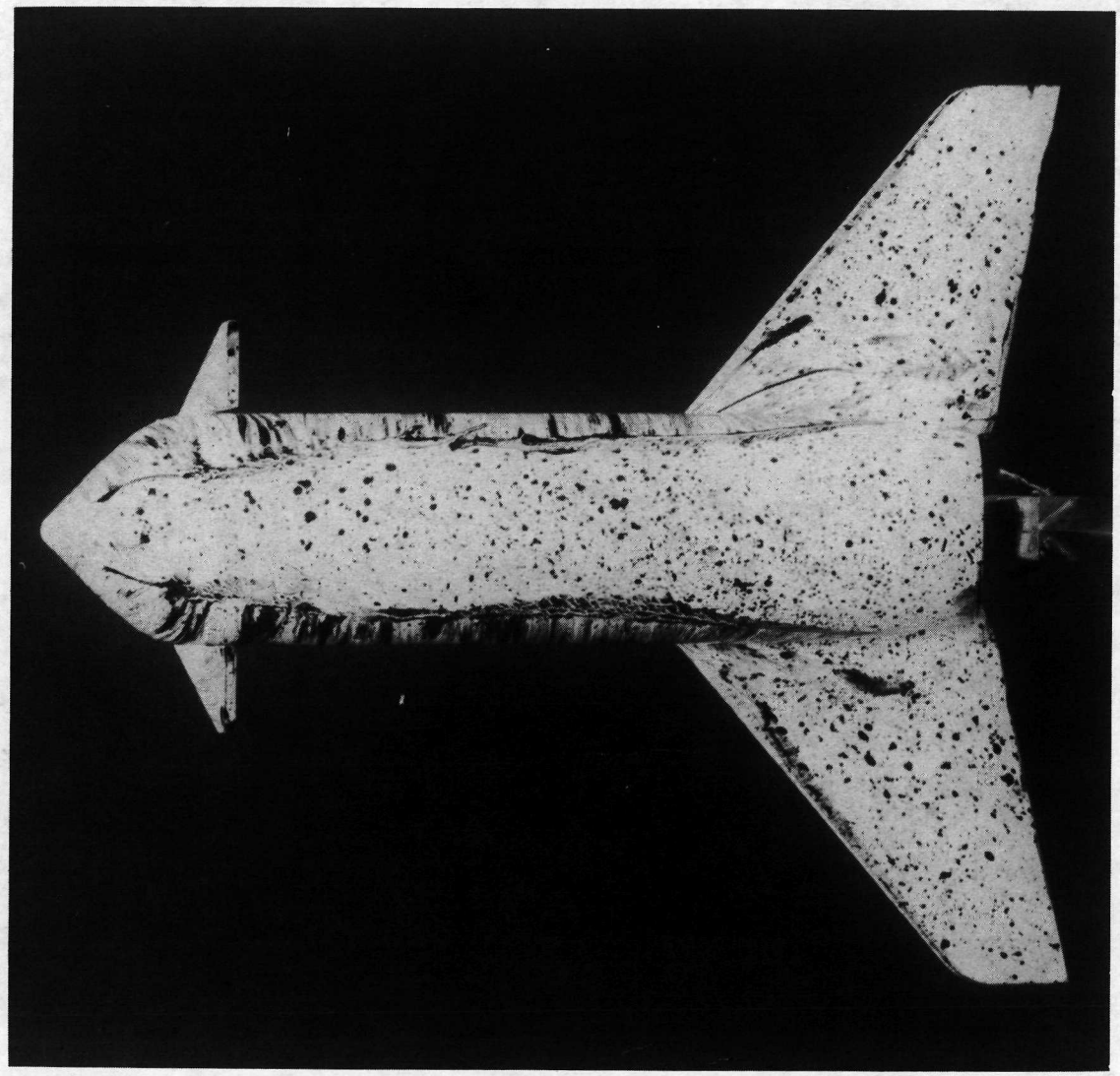

L-72-6538

(b) Top view.

Figure 16.- Continued.

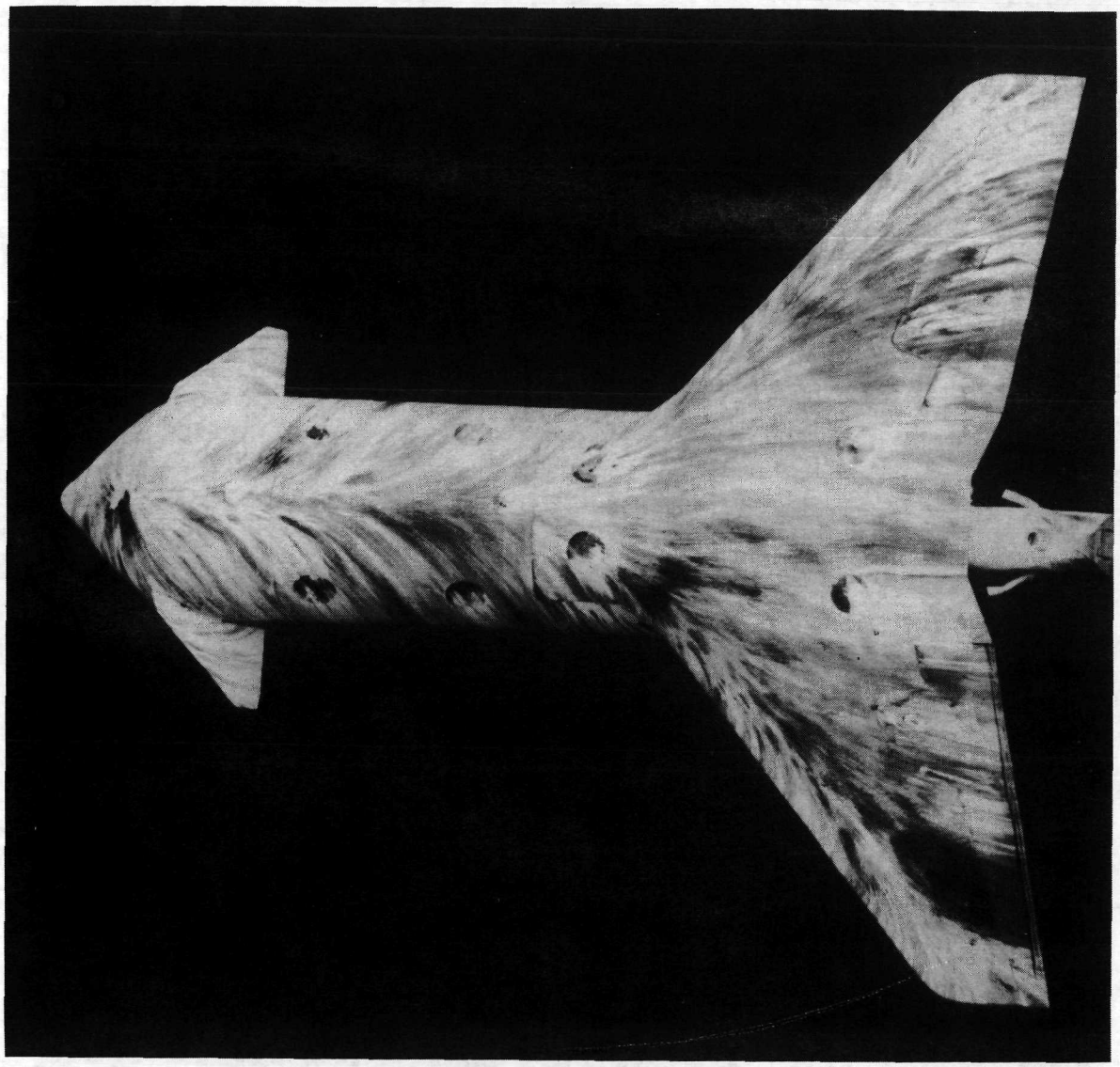

L-72-6539

(c) Bottom view.

Figure 16.- Concluded.

NASA-Langley, 1972 —— 31 L-8453

NATIONAL AERONAUTICS AND SPACE ADMINISTRATION
WASHINGTON, D.C. 20546

OFFICIAL BUSINESS
PENALTY FOR PRIVATE USE $300

SPECIAL FOURTH-CLASS RATE
BOOK

POSTAGE AND FEES PAID
NATIONAL AERONAUTICS AND
SPACE ADMINISTRATION
451

U.S.MAIL

POSTMASTER: If Undeliverable (Section 158 Postal Manual) Do Not Return

"The aeronautical and space activities of the United States shall be conducted so as to contribute . . . to the expansion of human knowledge of phenomena in the atmosphere and space. The Administration shall provide for the widest practicable and appropriate dissemination of information concerning its activities and the results thereof."

—NATIONAL AERONAUTICS AND SPACE ACT OF 1958

NASA SCIENTIFIC AND TECHNICAL PUBLICATIONS

TECHNICAL REPORTS: Scientific and technical information considered important, complete, and a lasting contribution to existing knowledge.

TECHNICAL NOTES: Information less broad in scope but nevertheless of importance as a contribution to existing knowledge.

TECHNICAL MEMORANDUMS: Information receiving limited distribution because of preliminary data, security classification, or other reasons. Also includes conference proceedings with either limited or unlimited distribution.

CONTRACTOR REPORTS: Scientific and technical information generated under a NASA contract or grant and considered an important contribution to existing knowledge.

TECHNICAL TRANSLATIONS: Information published in a foreign language considered to merit NASA distribution in English.

SPECIAL PUBLICATIONS: Information derived from or of value to NASA activities. Publications include final reports of major projects, monographs, data compilations, handbooks, sourcebooks, and special bibliographies.

TECHNOLOGY UTILIZATION PUBLICATIONS: Information on technology used by NASA that may be of particular interest in commercial and other non-aerospace applications. Publications include Tech Briefs, Technology Utilization Reports and Technology Surveys.

Details on the availability of these publications may be obtained from:

SCIENTIFIC AND TECHNICAL INFORMATION OFFICE

NATIONAL AERONAUTICS AND SPACE ADMINISTRATION

Washington, D.C. 20546